

The Anatomy of an Antibacterial Clay Deposit: A New Economic Geology

Keith D. Morrison,* Stanley N. Williams, and Lynda B. Williams[†]

School of Earth and Space Exploration, Arizona State University, Tempe, Arizona 85287-1404

Abstract

Argillic alteration zones associated with porphyry and epithermal deposits may contain clays that are antibacterial against antibiotic-resistant human pathogens, thus providing new economic potential for these deposits. This study examined the antibacterial activity of hydrothermal alteration zones in andesite porphyry and volcanoclastic rocks from a sulfur- and pyrite-rich clay deposit in the Oregon Cascades. The deposit is located along a fault zone west of Crater Lake, in Eocene-age volcanic rocks.

Mineralogical relationships were used to deduce emplacement temperatures of the antibacterial clays, and oxygen isotopes of secondary quartz were used to deduce fluid sources. High-sulfidation alteration from magmatic fluids (200°–300°C) produced highly illitic Black clay with elemental sulfur and up to 19 wt % pyrite. Low-sulfidation, mixed magmatic-meteoritic fluids (150°–200°C) produced pervasive Blue clay containing reduced Fe-bearing rectorite and minor pyrite (4–5 wt %). White clay containing smectite and kaolinite formed along faults from cooler ($\leq 100^\circ\text{C}$) meteoric water. Surficial Red clay contains illite-smectite and goethite from the oxidation of pyrite.

Antibacterial activity is greatest in the pyrite-bearing clays but the nonsulfide-bearing White clays also inhibit bacterial growth. Red oxidized clays are not antibacterial. When antibacterial clays are rehydrated in deionized water (100 mg/ml), the pH (<4.5) drives mineral dissolution and metal hydrolysis to produce Fe^{2+} , Al^{3+} , and hydroxyl radicals that kill bacteria. The pH and Eh of the hydrated clay is important for stabilizing these aqueous reactants, therefore we find no antibacterial effect where carbonates or goethite are stable. Accordingly, the antibacterial effect is diminished with burial depth (meters) where the Eh is too low to drive pyrite oxidation.

Introduction

Antibiotic resistant bacteria are a global health concern requiring new approaches to control their proliferation. One popular approach taken during the past 25 years has been the introduction of drugs derived from natural products (Newman and Cragg, 2007). Traditional antibiotics are organic molecules that inhibit DNA replication, protein, and cell wall synthesis (Walsh, 2000), and many pathogens (e.g., Methicillin-resistant *Staphylococcus aureus*; MRSA) subsequently develop antibiotic resistance. As a result, alternative therapies against bacterial infections have gained attention. Medicinal and therapeutic uses of clays have been documented for thousands of years (Carretaro, 2002) and have been extensively used topically, as digestive aids adsorbing intestinal toxins (Wilson, 2003; Ferrell, 2008) and in wound healing (Williams and Hillier, 2014). Despite the clear beneficial effects on human health related to ridding the body of infectious agents, the scientific basis for the antibacterial action of certain clays

has only recently been investigated (Haydel et al., 2008; Williams et al., 2008, 2011; Kibanova et al., 2009; Otto et al., 2010; Londoño and Williams, 2016; Morrison et al., 2014, 2016).

Clay, which is defined as a mineral assemblage of particles $< 2 \mu\text{m}$ in diameter (Moore and Reynolds, 1997), is formed in a variety of geologic settings, but only a few clays have been recognized as antibacterial (Williams et al., 2004, 2008, 2011; Morrison et al., 2014, 2016; Londoño et al., 2017). These clays are from hydrothermal deposits containing reduced Fe-bearing clay minerals associated with volcanism (Williams et al., 2008, 2011; Morrison et al., 2014). Morrison et al. (2016) presented evidence for the antibacterial mechanism of clay marketed by Oregon Mineral Technologies Inc. (OMT) as healing clay. It is also sold as an alkaline soil amendment because of its high sulfur content and acidity (Ferrero, 1992). We studied the mineralogical and geochemical makeup of the argillic alteration zones from the OMT deposit, focusing on the geologic environment that produces antibacterial clays. Sulfide deposits found globally, related to subduction zone volcanism, commonly exhibit argillic hydrothermal alteration and these are potential hosts for clays that may be effective at killing a broad spectrum of human pathogens, including those that have evolved antibiotic resistance (Williams et al., 2011;

[†] Corresponding author: e-mail, lynda.williams@asu.edu

* Present address: Biosciences and Biotechnology Division, Physical and Life Sciences Directorate, Lawrence Livermore National Laboratory, Livermore, California 94550; e-mail, morrison30@llnl.gov.

Morrison et al., 2014, 2016). The antibacterial clay assemblages studied here are from argillic alteration zones, which are commonly removed as mine tailings from these types of deposits and could be repurposed for medicinal applications, providing new economic value.

Brunet de Courssou (2002) brought attention to the antibacterial effect of clays on human pathogens by demonstrating the successful treatment of Buruli ulcer, a *Mycobacterial* infection that causes necrotizing fasciitis (flesh-destroying disease). Using a poultice made from the French Green clay and water (applied topically and changed daily), de Courssou cured more than 100 patients suffering from this infection that did not respond to antibiotics (Williams et al., 2004). The French Green clay used is a reduced Fe-rich clay dominated by illite-smectite (I-S) and thought to be related to volcanic activity in the Massif Central region of France (Williams et al., 2008).

Evaluation of nearly 100 clays sampled worldwide has identified <10% that are antibacterial or inhibitory to bacterial growth. The pH of aqueous suspensions of these clays (50 mg clay/ml water) is either >10 or <4.5 (Williams et al., 2011). The most effective antibacterial clays are those from hydrothermally altered volcanics (ash and pyroclastic materials) where reduced metals (e.g., Fe²⁺) are concentrated in hydrothermal waters. Aluminum is soluble at both high and low pH; therefore further research focused on the metals released from aluminosilicates and their role in the antibacterial process (Morrison et al., 2016; Londoño et al., 2017). This paper describes the mineralogy of the clay alteration zones in the OMT deposit, which consist of epithermal alteration by acidic to neutral, low to intermediate sulfur-rich hydrothermal fluids (as defined by Einaudi et al., 2003) that produced the most effective antibacterial clay we have identified. The OMT deposit is an undisturbed emplacement providing essential information about how the antibacterial clay assemblages formed. Understanding the mineralogical controls on the antibacterial process is key to discovering new antibacterial mineral deposits and evaluating their economic potential.

Geologic Setting

Hydrothermal ore deposits and porphyry alteration systems associated with subduction zones and arc volcanoes are found worldwide. These systems produce hydrothermal alteration of large volumes of rock as much as 3 km away from the intrusive heat source (Giggenbach, 1997; Singer et al., 2008; Mosier et al., 2009; Pirajno, 2009; Shanks and Thurston, 2012). Economically viable deposits of high-grade base and precious metals generally occur within 0.5 km of an intrusive body, and the hydrothermal alteration grades from potassic alteration proximal to the intrusion to distal phyllic and argillic alteration zones (Hedenquist and Lowenstern, 1994). The latter zones are composed primarily of clay minerals, quartz, and pyrite (Meunier, 2005).

The OMT clay deposit is located in the Cascade Mountains, (Douglas Co., Oregon) ~25 km west of Crater Lake. The deposit is part of the larger Cascade volcanic arc system that formed from the subduction of the Juan de Fuca plate beneath North America (Hammond, 1979; Sherrod and Smith, 2000; Bacon, 2008) and lies at the eastern edge of the Western Cascades (Fig. 1). The clay alteration occurred over the last 45 m.y. (Walker and MacLeod, 1991; Sherrod and

Smith, 2000). Most of the western Cascades was emplaced between 45 to 18 Ma with intermittent volcanic activity until ~8 Ma (Hammond, 1979). The High Cascades to the east of the deposit began to form at ~7 Ma, with Mount Mazama erupting 7,700 years ago, forming Crater Lake (Priest, 1990; Bacon, 2008).

Detailed geologic sampling of the deposit (Ferrero, 1992) revealed regional alteration of dacite and andesite to pyrophyllite, pyrite, and quartz along a major NW-SE-trending fault marked by the Foster Creek drainage. To the west, the OMT clay is capped by basalts associated with the Sardine Formation, which were extruded from 17 to 7 Ma (Sherrod and Smith, 2000), and to the east the deposit is bound by a N-S-trending fault zone aligned with the Rogue River drainage (Fig. 1A, B). This region is blanketed by pyroclastic and ash deposits from the eruption of Mount Mazama. Andesite lava flows from the Little Butte Volcanic Formation make up the bulk of the parent rock, ranging in age from 25 to 17 Ma (Walker and MacLeod, 1991; Sherrod and Smith, 2000). Zones of elemental sulfur are associated with hypabyssal intrusive rock (22–8 Ma). Recent glaciation (30–10 Ka) exposed the hydrothermally altered clay zones (Walker and MacLeod, 1991; Sherrod and Smith, 2000). The pyroclastics in the OMT deposit are much older (~30–25 Ma) than the deposits of Mount Mazama (Fig. 1C), but regional silicic volcanism over the last ~70 k.y. may have generated heat for the long-term hydrothermal alteration of the OMT volcanic parent materials (Bacon, 2008).

Samples

Field reconnaissance included mapping the distribution of clay alteration zones in the OMT deposit, and sampling for mineralogical analysis and antibacterial testing. Unaltered parent rock associated with each clay zone was sampled to identify the primary minerals subsequently altered to clay. A series of roads used for logging provided access to four sample locations where various clay alteration zones were identified and sampled (Fig. 1C). The sample locations are named Sulfur mine (formerly Last Chance mine), Open Pit, Foster Creek, and Road Cut. The area of the mineral leases is approximately 4,500 acres (18 km²) and reconnaissance drilling suggested that the thickness may be up to 600 m (Ferrero, 1992).

Fifty hand samples from the OMT field area were studied mineralogically and chemically. There are four major alteration zones associated with the deposit, which we have named by the dominant color of each clay: Red (oxidized), White (bleached), Blue (reduced Fe-rich), and Black (pyrite-rich, containing elemental sulfur). Antimicrobial testing was performed on each of the clay samples in order to correlate mineralogy and geochemistry with antibacterial effectiveness.

Sulfur mine: The surface clays in all sample sites are oxidized, producing a Red clay containing goethite. Blue clay in the Sulfur mine is found directly beneath the surficially weathered Red clay. Elemental sulfur is found only at the Sulfur mine sampling site, where it occurs as hand-sized crystals in veins. The sulfur is surrounded by Black sulfide-rich clay that grades outward to Blue clay (Fig. 2). Sulfur was mined at this location in the 1930s (Last Chance mine).

Open Pit: The OMT Open Pit exposes Red (oxidized) and White (bleached) clays overlying the dominant reduced

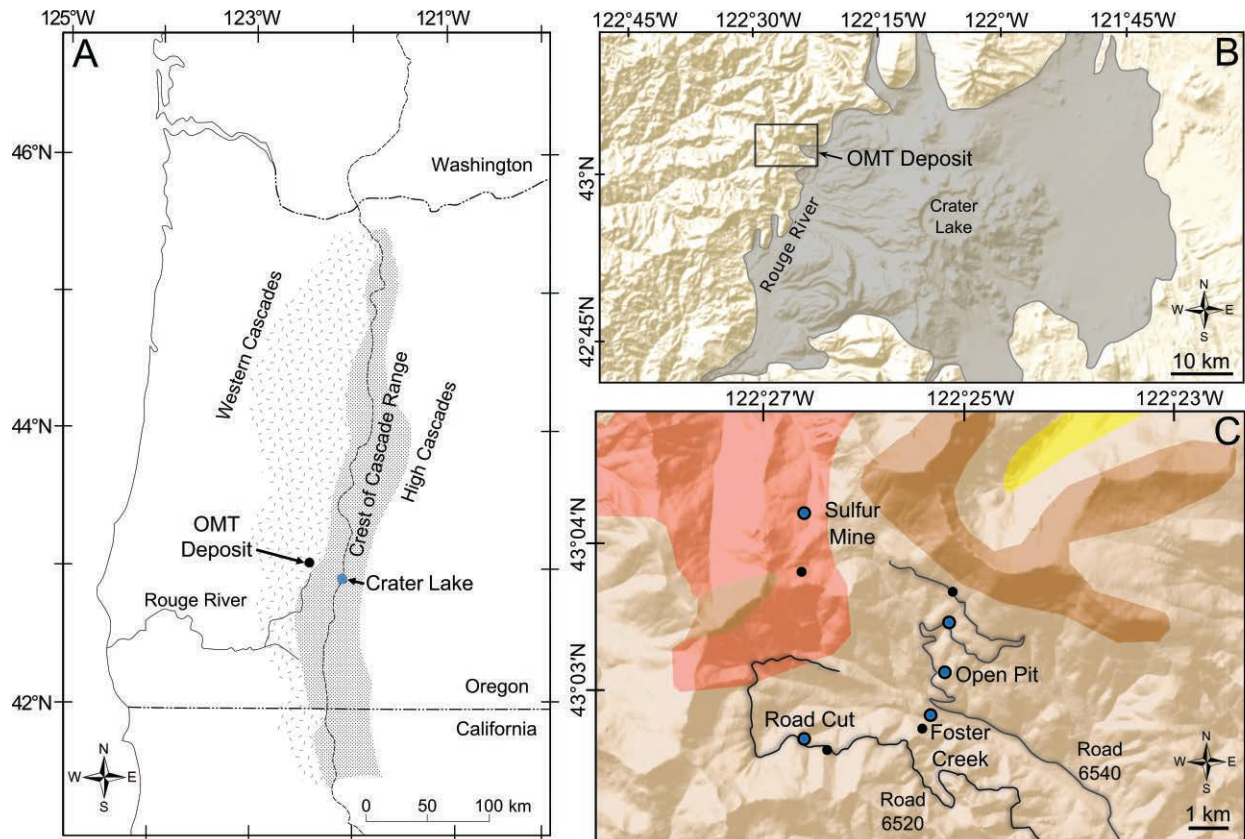


Fig. 1. Study area. (A). The OMT deposit is ~25 km northwest of Crater Lake in the Western Cascade Range. (B). Gray shaded area shows pyroclastic flows from the Mount Mazama eruption (Bacon, 2008). (C). Regional geology showing andesite (tan), hypabyssal intrusive rocks (red), basalts (brown), and younger glacial deposits (yellow) (from Sherrod and Smith, 2000). Sample locations are indicated by black dots (parent rock) and blue circles (clay samples).

Fe-rich Blue clay at depth (Fig. 3). Surface weathering produced the oxidized Red clay, whereas the White clay is located primarily in fault zones, where meteoric waters are active. The Red and White clay assemblages range in thickness



Fig. 2. Sulfur mine sample site. (A). Vein of elemental sulfur and Black clay (dotted outline), surrounded by Blue (right) and White (left) clay zones. (B). Close-up of sulfur crystals in the dominant Blue clay, with red oxidized surface.

from 3 to 9 m in the Open Pit. Postalteration minerals (gypsum, iron oxides) are found in these zones, presumably from the oxidation of pyrite, which is a minor constituent of the Blue clay. The parent rock of the Blue clay is hydrothermally altered andesite porphyry and pyroclastic material. Stockwork is exposed in the Open Pit and comprises veins dominated by quartz and pyrite.

Hydrothermal alteration and weathering exposed in the Open Pit form these distinct clay assemblages that represent variations in oxidation conditions and pH (Morrison et al., 2014).

Foster Creek and Road Cut: The Blue clay assemblage dominates at the Foster Creek sampling site with a well-defined layer of oxidized Red clay on top. Blue clay is also exposed in the Road Cut sampling site along Forest Service road 6520 to the southeast of Foster Creek (Fig. 1C). This clay appears to be associated with a fault, and the alteration zone extends ~10 m. Samples were collected at 0.3-m intervals across this exposed fault zone.

Methods

Mineralogy and geochemistry

X-ray diffraction: X-ray diffraction was performed using a Siemens D5000 diffractometer (ASU LeRoy Center for Solid State Science) with CuK_α radiation. Bulk samples (5 g) were

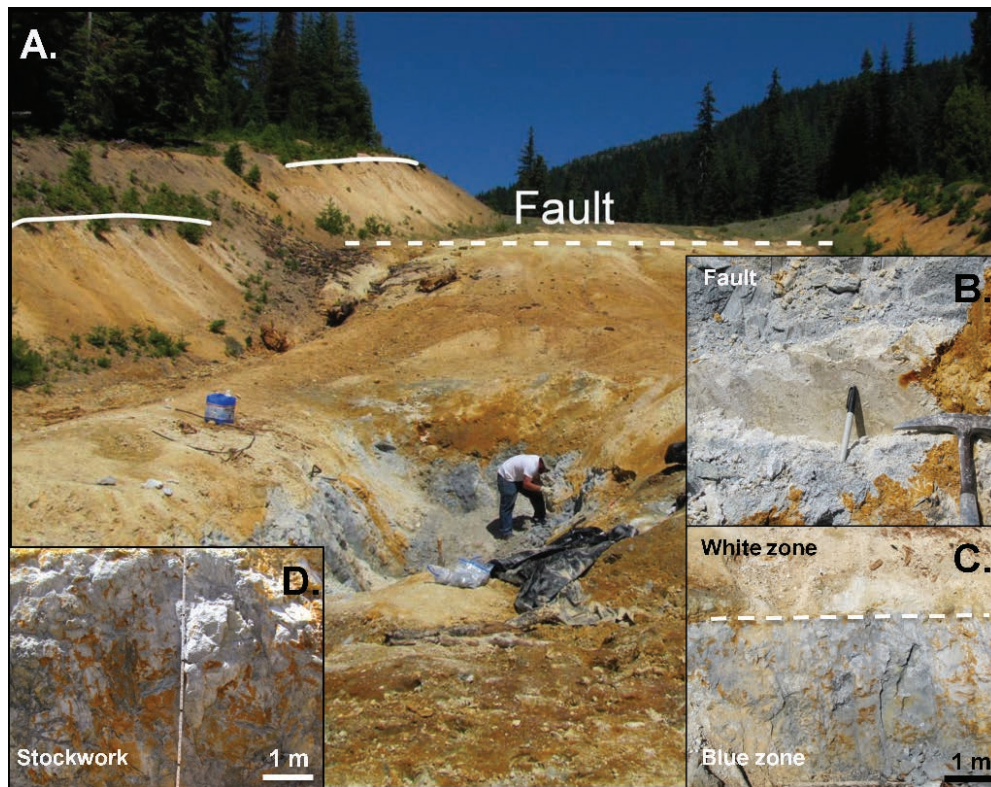


Fig. 3. The Open Pit provides the best exposure of the antibacterial Blue clay assemblage that dominates the OMT deposit. (A). Northwest-southeast faults are present throughout the Open Pit where the surficially oxidized Red clay is not antibacterial. (B) and (C) insets show White clay that overlies the Blue clay and is associated with faults. (D). Stockwork of hydrothermal quartz and pyrite.

lightly disaggregated, then placed in 50 ml of deionized water (DIW) water, and ultrasonicated in a Braun disaggregator for 1 min to disperse the clay minerals. Samples were rinsed free of salts until the clays were dispersed. Clay fractions ($<2.0 \mu\text{m}$) were separated using standard procedures (Jackson, 1979). The clays were Na saturated, using 1N NaCl, and then transferred to dialysis tubing (3500 Dalton molecular weight cut-off), where they were rinsed with deionized water (DIW) to remove chloride. Oriented clay mounts were prepared by pipetting a clay suspension ($\sim 20 \text{ mg/ml}$) onto a glass slide so that the water surface tension orients clay platelets parallel to the slide when air-dried. The oriented clay slides were then saturated with ethylene glycol vapor at 60°C overnight (Moore and Reynolds, 1997). X-ray diffraction patterns of mixed-layered clay minerals were calculated using Sybilla modeling software (McCarty, 2009). The Reichweite, (R) is the degree of nearest neighbor (unit cell) ordering of mixed-layered illite-smectite (I-S) and this value increases with degree of illitization as a function of temperature. The term R0 refers to random ordering of I-S (low temperature), and R3 refers to ISII ordering at higher temperature ($200^\circ\text{--}300^\circ\text{C}$), depending on heat duration (Moore and Reynolds, 1997).

Bulk samples prepared for quantitative random powder XRD followed procedures recommended by Eberl (2003). Samples were gently crushed and passed through a $250\text{-}\mu\text{m}$ sieve. Sieved samples were spiked with 25 wt % $\alpha\text{Al}_2\text{O}_3$ as an internal standard and micronized in ethanol, using a

McCrone Mill, and dried at 60°C overnight (Srodon et al., 2001). The micronized samples were then saturated with Verrel® to promote random orientation, sieved, and side-loaded into an XRD mount. All powdered samples were analyzed on a Siemens D-5000 XRD ($\text{CuK}\alpha$ radiation), using a scintillation detector with 1° divergence and receiving slits, scanning from 5° to 65° at $0.02^\circ 2\theta$ steps with a 2 s/step count time. The quantitative mineralogy was calculated using the full pattern peak-fitting program RockJock 11 (Eberl, 2003). The degree of fit between the measured and calculated XRD pattern was determined using equation (1). Clay XRD patterns were fit using diffraction angles from 19° to $64.5^\circ 2\theta$ and all degrees of fit were <0.1 , which corresponds to a $>95\%$ convergence of the fit.

$$\text{Degree of fit} = \Sigma \frac{(\text{Measured} - \text{Calculated})^2}{\text{Calculated}} \quad (1)$$

X-ray fluorescence: Elemental analysis was performed on borate glass fusions of bulk rock samples (Baedecker, 1987), using a Siemens SRS 300 AS XRF spectrometer (USGS, Boulder, CO). Samples (2 g) were heated to 925°C for 2 h, cooled, and mixed with lithium tetraborate-metaborate (66% tetraborate, 33% metaborate) in a 1/10 ratio. Borate glass fusions were prepared using an automated XRF fusion machine (XRF Scientific). Samples were transferred to platinum/gold crucibles and progressively heated to $1,100^\circ\text{C}$ under constant

mixing and poured into casting molds to cool. All nonvolatile major element oxides were calibrated with reference standards and totaled 97 to 98%.

Leachate chemistry ICP-MS: Because the aqueous leachates of the antibacterial clay poultices exhibited bactericidal activity within 24 h (Williams et al., 2004), we analyzed the chemistry of the clays equilibrated 24 hrs with DIW, using inductively coupled plasma mass spectrometry (ICP-MS). Aqueous leachates of clay were prepared by ultra-sonicating 100 mg/ml of bulk clay samples with DIW (1 min), followed by shaking (24 hrs) to chemically equilibrate to the same degree used in medicinal applications. To separate leachates from the minerals, the suspension was centrifuged (13,000 rpm, 1 h). Because of the salinity of the leachates, the minerals form aggregates so this centrifugation removes most nanoparticles. Elemental analyses of the aqueous leachates were performed using a Thermo X-Series quadrupole ICP-MS (W.M. Keck Laboratory for Environmental Biogeochemistry at ASU). Samples were acidified with 2% nitric acid, prior to analysis. Dilutions of 1/10 and 1/100 were analyzed along with undiluted samples and calibrated to multielement reference standards (EPA method 200.8). Elemental concentrations were determined for Na, Mg, Al, P, K, Ca, Ti, V, Cr, Mn, Fe, Co, Ni, Cu, Zn, As, Se, Rb, Sr, Mo, Cd, Cs, Ba, Hf, W, Ag, Hg, Pb, and U. Certain elements (e.g., Si and S) are not ionized efficiently by ICP-MS or have interferences, and therefore were not included in the analyses.

Ferric and ferrous iron assay: Mineral leachates were measured for Fe^{2+} , Fe^{3+} , and total Fe immediately after centrifugation to remove minerals, using a phenanthroline method modified from Anastácio et al. (2008). The measurement of Fe^{2+} was performed under red photographic bulbs to prevent the photochemical reduction of the binuclear Fe^{3+} -phenanthroline complex to the Fe^{2+} -phenanthroline complex (Komadel and Stucki, 1988). For the measurement of Fe^{2+} a 10- to 200- μL aliquot of leachate was added to 0.5 ml of 2.5 wt % 1,10 phenanthroline (dissolved in 95% ethanol). The solutions were then diluted with 1 wt % sodium citrate to a final volume of 1.5 ml. Absorbance was measured with a spectrophotometer at a 510-nm wavelength after 15 min for color development. Measurement of Fe^{3+} was achieved in a similar manner using 200 μL of 10 wt % hydroxylamine hydrochloride as the reducing reagent. Stock solutions of ferrous ammonium sulfate hexahydrate and ferric chloride (200 mg/l) were prepared and acidified using 3.6 N sulfuric acid, producing linear calibrations at concentrations ranging from 1 to 8 mg Fe/L.

Hydrogen peroxide assay: H_2O_2 concentrations were measured in mineral suspensions (100 mg/ml) reacted with *E. coli* growing in 10 g/L Luria Broth (LB). The assay for H_2O_2 described by Cohn et al. (2005) was modified for work with clays. Aliquots of the bacteria-mineral suspensions were sampled after 4 hrs of incubation at 37°C and centrifuged at 13,000 rpm (Sorvall RC-5b) for 2 min. Then 20 to 500 μl of the supernatant liquid was transferred into microcentrifuge tubes containing a buffer solution (1M KH_2PO_4 and 50 mM EDTA, pH 4.2), to a final volume of 1,400 μl . A 50- μl aliquot of 5 mM leuco crystal violet was added followed by 50 μl of horseradish peroxidase type II (14.4 enzyme units/ml). Absorbance was measured with a spectrophotometer at 590-nm

wavelength after 15 min for color development. Hydrogen peroxide calibration curves ranging from 0.5 to 25 μM were prepared in the same manner.

Eh and pH measurements: All Eh and pH values were measured using an Orion Dual Star meter (LE501 ORP and LE409 pH electrodes). The platinum Ag/AgCl (4 M KCl) Eh electrode was calibrated using Zobel solution resulting in a +220 mV offset with respect to a standard hydrogen electrode (Nordstrom, 1977).

Speciation modeling: Stability diagrams for the Fe-S-O-H, Al-S-O-H, and S-O-H systems were calculated using the MEDUSA program (Puigdomenech, 2004). Stability fields were calculated from infinite dilution up to the concentrations of Fe and Al (~2 mM) measured in bactericidal samples of the OMT Blue clay leachates after 24 hrs. The generated stability field represents an approach to equilibrium. The anions in the OMT Blue clay aqueous leachates are dominated by sulfate (Williams et al., 2011). Sulfate concentrations (mM) were ~2 times greater than those of Fe, so this ratio was used for the calculations.

Secondary ion mass spectrometry: Microanalysis of $\delta^{18}\text{O}$ isotope ratios in secondary quartz associated with the various clay assemblages was performed to evaluate the sources of hydrothermal fluid (magmatic or meteoric) that produced the alteration products. The clay size fraction (<2 μm) was removed from samples to concentrate the coarse secondary quartz disseminated throughout the alteration zones. Bulk samples were dispersed in DIW and disaggregated using a Braun ultrasonifier. The suspended clays were decanted and the sedimented fraction was air-dried. Quartz crystals were selected under a petrographic microscope and epoxy grain mounts were made using a low volatile epoxy (Buehler Epoxy-Cure) and polished to ~1- μm flatness. The mounts were rinsed in a sonic bath with DIW to remove polishing material, dried at 60°C and Au coated for charge compensation during solid-state isotope analysis.

Oxygen isotope measurements were made using a Cameca IMS 6f secondary ion mass spectrometer (SIMS) in the National SIMS facility at Arizona State University. Microanalyses of oxygen isotopes in quartz were performed according to the SIMS methods of Hervig et al. (1992, 1995), which are optimized for measuring oxygen isotopes in silicate minerals. A 10-kV Cs^+ ion beam with a 10- to 25-nA current was focused into a 20- to 40- μm spot for analysis of the polished quartz grains. The positive charge buildup from Cs^+ ion bombardment of the quartz surface was offset by the use of a normal incidence electron gun, which focuses high-energy electrons on the sample surface for charge compensation (Hervig et al., 1992). The spectrometer was set to a mass resolving power ($\Delta M/M$) ~2,100 to eliminate mass interferences. In addition, extreme energy filtering of the negative secondary ions ($^{18}\text{O}^-$ and $^{16}\text{O}^-$) sputtered from the quartz was achieved by reducing the sample voltage 350 eV, which allows only high-energy secondary ions (>350 eV) to enter the mass spectrometer; eliminating interferences from most molecular ions (Hervig et al., 2006). The combination of extreme energy filtering and mass resolving power used provides ion yields high enough to achieve precision of each analysis around $\pm 1.4\%$ 1σ . The standard error for multiple measurements of a single crystal (4–8 analyses) is <1% 1σ .

All $^{18}\text{O}/^{16}\text{O}$ ratios were standardized to the $^{18}\text{O}/^{16}\text{O}$ ratio of standard mean ocean water (SMOW; 2.0052E-3) and verified using an internal quartz standard (Arkansas quartz, $^{18}\text{O}/^{16}\text{O}$ 2.0423E-3; Baertschi, 1976). Quartz standard $^{18}\text{O}/^{16}\text{O}$ ratios were measured before and after analysis of unknowns to correct for instrumental drift (Hervig et al., 2006). All oxygen isotope ratios are expressed using standard delta (δ) notation (eq. 2), and reported in parts per thousand (‰) (Faure, 1998).

$$\delta = \left(\frac{R \left(\frac{\text{O}^{18}}{\text{O}^{16}} \right) \text{Sample}}{R \left(\frac{\text{O}^{18}}{\text{O}^{16}} \right) \text{Standard}} - 1 \right) \times 1,000\text{‰} \quad (2)$$

Microbiology

Disk diffusion: A qualitative disk diffusion method was initially used to screen the large sample set (>75 samples) from different alteration zones for antibacterial effectiveness. Antibacterial zones of inhibition were measured by a modification of the Kirby-Bauer disk diffusion method of antibacterial testing (Bauer et al., 1966) as follows. The antibacterial activity of each sample was determined by testing against antibiotic susceptible and resistant strains of gram-positive and gram-negative bacteria: *Escherichia coli* (ATCC 25922), β -lactam resistant *Escherichia coli* (ATCC 35218), *Staphylococcus epidermidis* (ATCC 14990), methicillin-resistant *S. epidermidis* (MRSE) (ATCC 35948).

Antibiotic susceptible strains (ATCC 25922 and 14990) were incubated (37°C) in Luria Broth (LB, 10g/ml) to log-phase growth using a rotary shaker (200 rpm). The population was adjusted to $\sim 10^8$ CFU/ml using fresh LB before plating. Antibiotic resistant strains were grown for 48 h at 30°C without shaking in order to establish biofilms. After 24 h, LB was removed from the culture tubes by pipette and a fresh aliquot of media was added. After 48 hrs, planktonic cells were decanted and biofilms were scraped from the sides of the tube, shaken on a vortex mixer for 2 min, then diluted to $\sim 10^8$ CFU/ml before plating. Next, 100 μl of culture was spread over LB agar plates and four 8-mm diam \times 4-mm deep wells were punched into the LB agar, using a flame-sterilized brass tube.

Bulk mineral samples (<250 μm) were steam autoclaved (121°C, 15 psi, 30 min) to sterilize. Mineral suspensions (100 mg/ml) were prepared and ultrasonicated for 1 min to disperse the clays. The wells in the inoculated LB agar plates were filled with 200 μl of this mineral suspension and incubated (37°C) for 24 h. Antibacterial elements leached from the clays diffuse into the agar creating a zone of growth inhibition that can be quantified by measuring the diameter (mm) of the zone of growth inhibition. Each sample was analyzed in quadruplicate. Samples that showed a zone of growth inhibition by disk diffusion were further evaluated using cell

viability plating (standard plate counting; National Committee for Clinical Laboratory Standards (NCCLS), 2005) to determine if cell death or growth inhibition occurred.

Bacterial viability plate counting: Colony forming units (CFU/ml) of bacteria were counted for *E. coli* ATCC 25922 and *S. epidermidis* ATCC 14990, using modified antibacterial susceptibility methods (Miles and Misra, 1938; Hedges, 2002). Mineral suspensions (200 mg/ml DIW) were then prepared and ultrasonicated for 1 min. Clays and bacteria were mixed in a 1/1 ratio diluting the mineral concentration by half (100 mg/ml in 10 g/L LB containing bacteria CFU $\sim 10^8$). Samples were incubated in a 96-well plate for 24 hrs on an orbital shaker. Serial dilutions of the samples (diluted by orders of magnitude down to 10^{-7}) were plated in aliquots of 10 μl onto LB agar plates in quadruplicate and incubated at 37°C for 24 h. Colony-forming units were then counted using a magnified backlight. Growth inhibition values were defined by a 10^3 CFU/ml reduction in cells. Samples were considered bactericidal only if they killed 100% of cells in the undiluted sample.

Results

Mineralogy

Parent rock: None of the parent rocks showed any antibacterial effect. However, we studied their mineralogy because identification of the alteration phases in the parent rock can aid in the interpretation of alteration temperature. The hydrothermal alteration of volcanic rock is governed mainly by the temperature and composition of the fluid reacting with the parent rock to produce alteration products (Velde, 1995). Porphyritic andesites are pervasive throughout the OMT deposit and appear to be the main parent rock that was hydrothermally altered in all sample sites. Previous studies identified hypabyssal intrusive rocks associated with the Sulfur mine containing more mafic parent rock in the deeper parts of the system (Power et al., 1981; Fiebelkorn et al., 1983). The parent andesite was sampled outside of the Open Pit, in the FS 6540 Road Cut, on the North side of the Foster Creek drainage (Fig. 1C). The Open Pit and Road Cut andesites contain higher Al_2O_3 and Na_2O contents than the Foster Creek and Sulfur mine parent rocks. The Sulfur mine parent rock has a more mafic composition with higher Fe, Mg, and Ca contents than the other sites sampled (Table 1).

The original andesitic parent-rock composition, dominated by plagioclase, contains secondary zeolites, quartz, chlorite, and smectite (Fig. 4). At the Sulfur mine, the parent rock shows little alteration of the plagioclase feldspar, with more intense hydrothermal activity focused along fractures/veins in the pervasive Blue clay. In the Open Pit, the parent andesite porphyry contains minor smectite, chlorite, laumontite, and

Table 1. Elemental Analysis of Parent Rock Samples Determined by XRF as Wt % Oxides (FeO* represents total Fe)

Sample	SiO ₂	Al ₂ O ₃	Fe ₂ O ₃	MgO	CaO	K ₂ O	Na ₂ O	TiO ₂	MnO	P ₂ O ₅	Total
Sulfur mine	49.97	17.97	10.09	6.15	9.19	1.35	0.9	1.21	0.13	0.41	97.37
Open Pit	58.48	19.16	6.61	2.75	5.84	1.58	2.99	0.79	0.08	0.16	98.44
Foster Creek	56.97	17.97	6.09	3.15	8.19	1.35	1.9	1.2	0.13	0.41	97.36
Road Cut	56.59	19.29	6.95	2.42	8.48	1.27	2.52	0.93	0.14	0.22	98.81

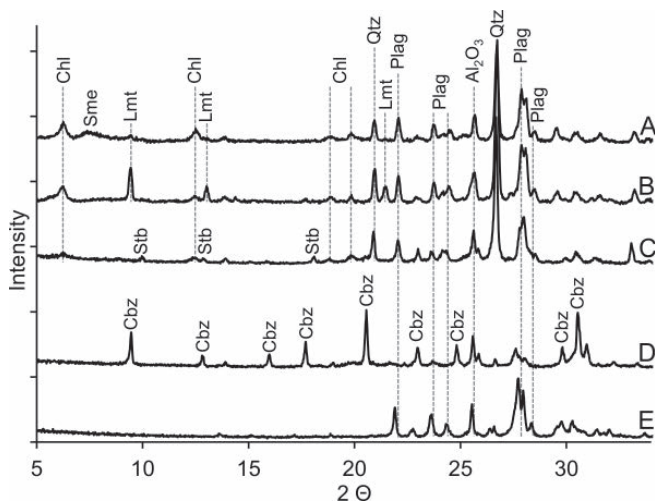


Fig. 4. Parent-rock X-ray diffraction patterns associated with (A, B) Open Pit, (C) Foster Creek, (D) Road Cut, and (E) Sulfur mine. Hydrothermal alteration minerals include quartz (Qtz), chlorite (Chl), laumontite (Lmt), stilbite (Stb), chabazite (Cbz), and smectite (Sme). Plagioclase (Plag) is a primary mineral.

unaltered plagioclase feldspars (andesine, oligoclase). The Foster Creek parent rock andesite contains quartz, stilbite, and oligoclase, whereas andesite from the Road Cut site contains chabazite. The alteration minerals formed in the parent-rock samples are characteristic of low-temperature hydrothermal alteration at near-neutral pH (Velde, 1995; Meunier, 2005). Figure 5 indicates the thermal stability ranges of the alteration minerals in the parent rock (Reyes, 1990; Velde, 1995).

Clay mineralogy

Sulfur mine: The Black clay, found only at the Sulfur mine, contains illite-smectite (I-S; 75% illite; $R > 1$) in S-bearing veins, grading to Blue clay toward the wall rock, which contains randomly ordered I-S (20% illite; R_0 ordered), indicating a lower temperature. Minor amounts of kaolinite and pure smectite are found in the less altered parent rock possibly from weathering by meteoric fluids (Fig. 6). Samples from the Sulfur mine location came from veins of hand-sized sulfur crystals surrounded by Black clay composed of I-S (75% illite; R_1 ordered) and smectite grading outward to Blue clay (Figs. 2, 6 B-C).

Open Pit: The Open Pit displays a series of northwest-southeast faults where White clay transects the massive Blue clay

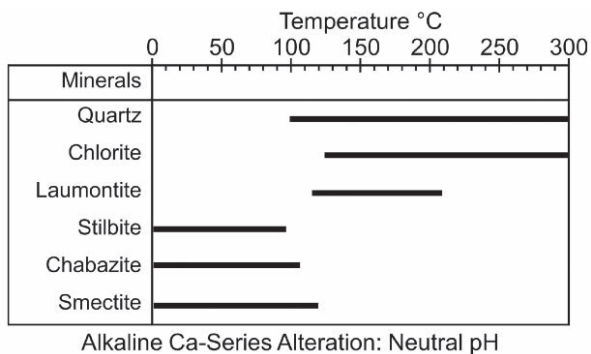


Fig. 5. Temperature stability ranges for parent-rock alteration minerals (Reyes, 1990; Velde, 1995).

(Fig. 3). Slickensides (Fig. 3B) related to faulting are found in this White clay assemblage, providing a path for meteoric water to oxidize and leach elements along these fracture zones. Rectorite (I-S with 55% illite; R_1 ordered) is pervasive in the Open Pit Blue clay, indicating temperatures up to 200°C (Velde, 1995). Some Blue clay zones contain more illitic I-S (70–80% illite), suggesting a higher temperature or a longer duration of heating (Meunier, 2005). The R_1 -ordered I-S gives rectorite a greater temperature stability range compared to I-S with lower illite content (Velde, 1995). It is also possible that the smectite layers of the rectorite play an important role in the antibacterial process (see “Discussion”).

Foster Creek and Road Cut: Samples from Foster Creek contain I-S (70% illite; $R > 1$ ordered), together with kaolinite and a minor amount of pure smectite (Fig. 6D-E). The formation of kaolinite indicates more acidic alteration at temperatures $< 250^\circ\text{C}$ (Reyes, 1990; Velde, 1995). The Blue clay from the Road Cut (Fig. 6F) contains 85% illite in I-S with R_3 ordering, indicating higher temperatures in this region south of the Open Pit. The presence of I-S, kaolinite, and pyrite at this location associated with faulting, suggests a short-lived alteration event with higher temperature moderately acidic fluids ($< 250^\circ\text{C}$; Reyes, 1990).

Oxygen isotopes

Quartz is not a component of basaltic to andesitic rocks, yet the clay alteration zones contain abundant secondary quartz. The oxygen isotope composition of the secondary quartz can reflect the source of fluid from which it precipitated. The interpretation of the quartz $\delta^{18}\text{O}$ values is dependent on both the water oxygen isotope composition and temperature of mineralization. Using mineralogical constraints such as the %I in I-S and stability fields for alteration minerals identified in the parent andesites (Fig. 5), we estimated the temperatures that affected each mineral assemblage (Beaty and Hugh, 1988; Hervig et al., 1995; Taylor and Huston, 1998; Binde-man, 2008). Using the well-established quartz-water $\delta^{18}\text{O}$ fractionation equation (Clayton et al., 1972) and the temperature indicated by mineral stability, we calculated the $\delta^{18}\text{O}$ composition of the water that would have been in equilibrium with the precipitated quartz, allowing an interpretation of the fluid source (magmatic vs. meteoric).

Secondary quartz is ubiquitous in all of the clay alteration zones, but the different textures of quartz (Fig. 7) are an indicator of whether the quartz precipitated as amorphous grains, or as a replacement of primary plagioclase. In either case, dissolution/precipitation requires the presence of water; therefore we can assume equilibration of oxygen isotopes between the water and the quartz. Figure 8 shows the results of the oxygen isotope measurements by SIMS on secondary quartz from the Black, Blue, and White clay alteration assemblages.

Antibacterial correlations with mineralogy

The antibacterial effectiveness (Figs. 9, 10) of each clay alteration zone was compared with the mineralogy to determine if a distinct mineral assemblage caused bactericide. The antibacterial effects of mineral samples tested against the two model bacteria (*E. coli* and *S. epidermidis*) are expressed here as bactericidal (killing 100%), inhibitory (reducing growth over

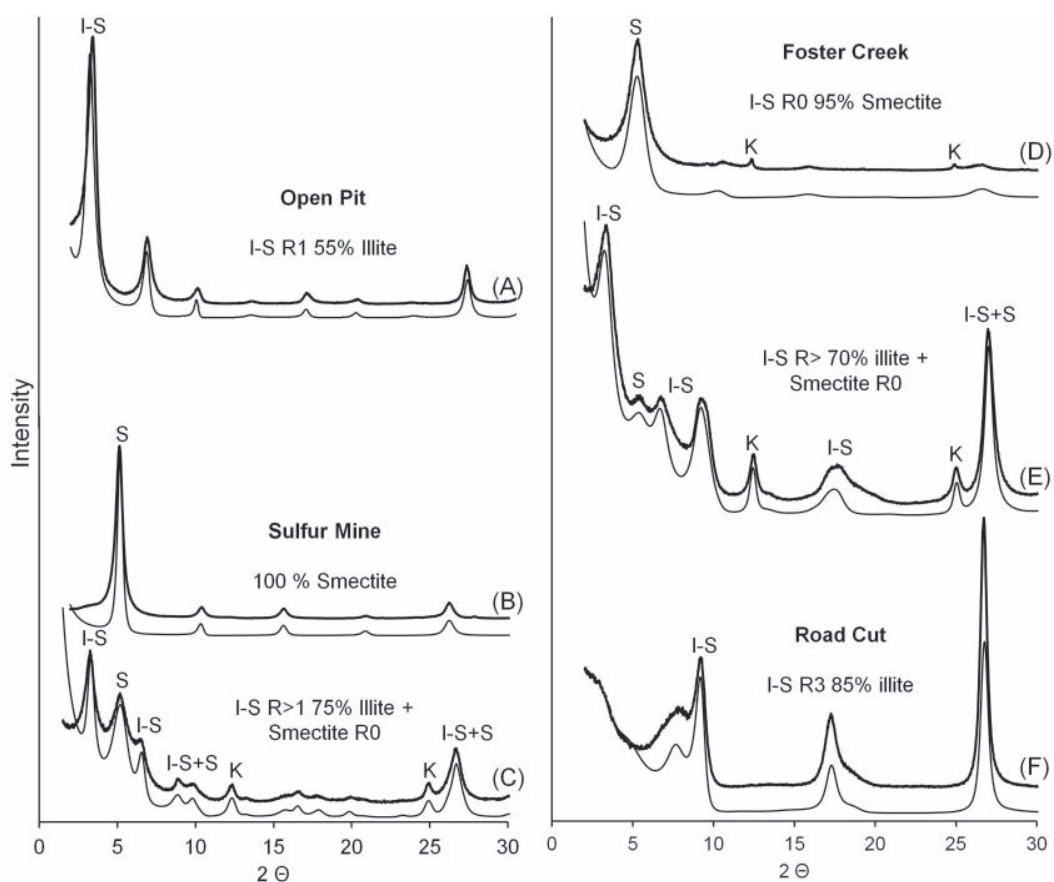


Fig. 6. Oriented clay XRD patterns (ethylene glycol saturated; Cu $k\alpha$ radiation). Bold patterns (top) are measured; thin lines are modeled. (A). Open Pit rectorite. (B). Sulfur mine White clay. (C). Sulfur mine Black clay. (D). Foster Creek White clay. (E). Foster Creek Blue clay. (F). Road Cut Blue clay. Mineral abbreviations: chlorite = (Chl), illite-smectite = (I-S), kaolinite = (K), smectite = (S), (from Morrison, 2015).

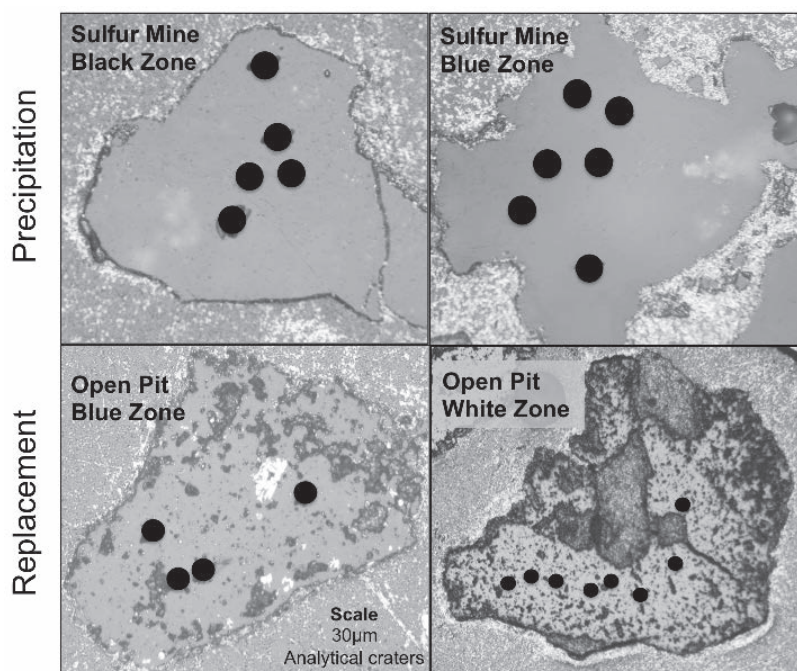


Fig. 7. Textural comparison of secondary quartz from (top) Sulfur mine, where it occurs as homogeneous precipitates, (bottom) the Open Pit where it shows replacement textures. Black dots depicting SIMS analytical craters are 30 μm .

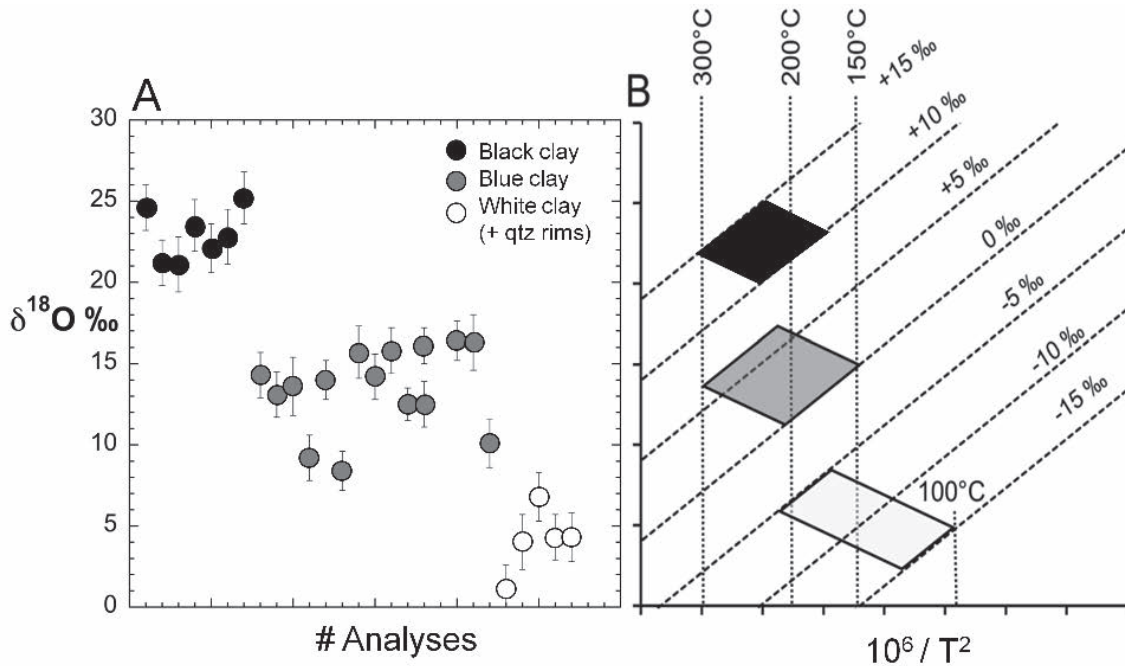


Fig. 8. Oxygen isotope ranges of secondary quartz from the OMT clay alteration assemblages. (A). The $\delta^{18}\text{O}$ composition of quartz from the Black, Blue, and White clay assemblages. (B). O isotope compositions calculated for water (dashed lines; +15 to -15‰) based on the quartz-water fractionation equation (Clayton et al., 1972) with temperature estimates from mineralogical stability fields.

three orders of magnitude), or nonantibacterial (no effect on growth).

Sulfur mine: Veins of elemental sulfur are abundant in the Sulfur mine sample site, and the Black clay that surrounds the sulfur crystals is I-S (75% illite; R > 1 ordered) containing finely disseminated pyrite (10–19%). The Blue clays adjacent to the Black clay (Fig. 11) contain a mixture of I-S that transitions

to pure smectite and plagioclase feldspar lower temperature alteration at the parent-rock contact. The parent rock contains minor precipitates of dolomite and calcite (1–2 wt %), which requires a higher pH for stability than the observed kaolinite (1–5 wt %), which is generally stable at pH < 5 (Table 2). This

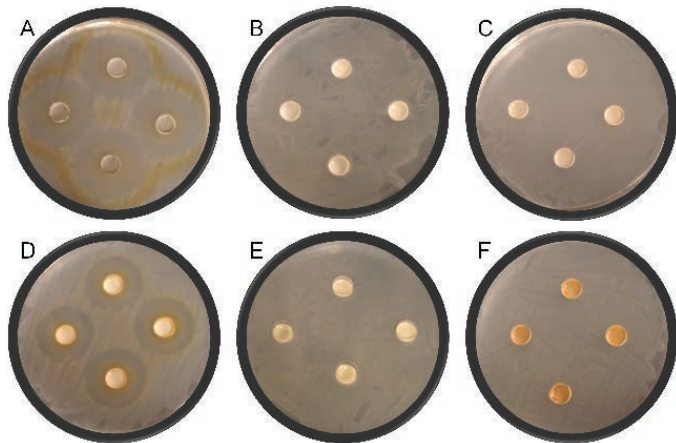


Fig. 9. Example of antibacterial zone of inhibition testing on LB agar plates growing *E. coli* (ATCC 25922). (A). Sulfur mine sample S7 (13 wt % pyrite) produced a 25-mm zone of growth inhibition. (B). Sulfur mine sample S1 (4.6 wt % pyrite and 5.5 wt % dolomite) showed no zone of inhibition. (C). Foster Creek sample F3 (4.8 wt % pyrite and 3.6 wt % calcite) showed no zone of inhibition. (D). Open Pit Blue clay sample P4 (4.4 wt % pyrite) generated a 16.2-mm zone of inhibition. (E). Open Pit White clay sample P2 (no measurable pyrite) showed no detectable zone of inhibition but inhibited growth according to plate counts. (F). Open Pit Red clay sample P1 (no pyrite, 3.4 wt % goethite) showed no zone of inhibition.

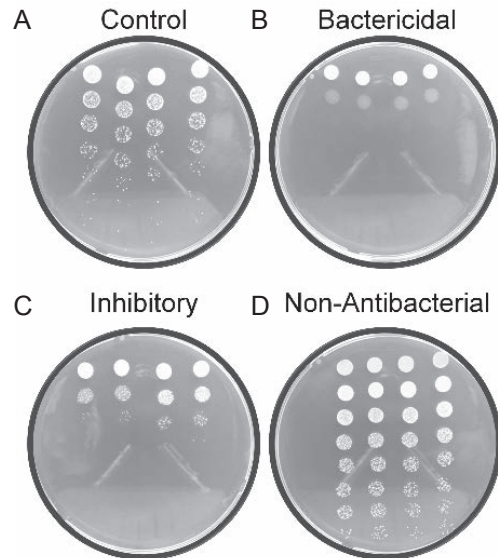


Fig. 10. Examples of plate counting bacterial colony forming units (CFU) to measure antibacterial effects. (A). Control *S. epidermidis* grown without clay, plated on LB agar and incubated (37°C, 24 hrs). (B). *S. epidermidis* incubated with antibacterial clay shows no growth (undiluted clay suspensions at top). (C). If CFU are fewer than the control, the clay is considered inhibitory to bacterial growth (cell density = CFU/dilution factor \times volume of fluid plated). (D). Oxidized Red clay showing no effect on bacterial growth.

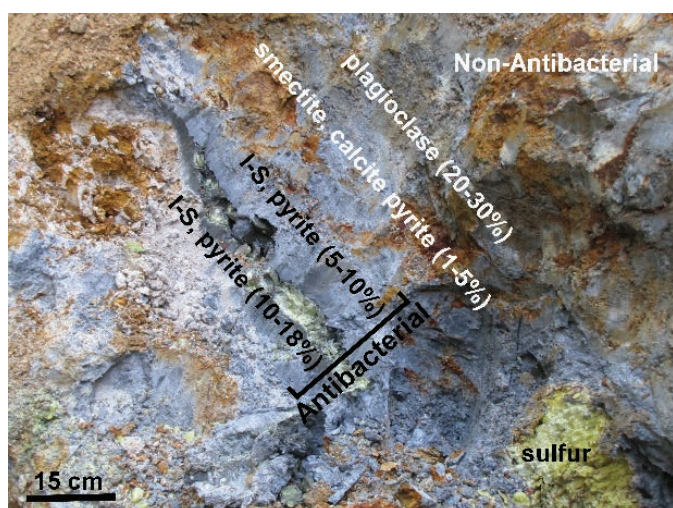


Fig. 11. Antibacterial correlation with mineralogy in the Sulfur mine samples. Sulfur crystals (nonantibacterial) are surrounded by antibacterial Black clay (9–18 wt % pyrite), antibacterial Blue clay (4–6 wt % pyrite), and nonantibacterial wall-rock alteration containing plagioclase, smectite, calcite, and minor pyrite.

supports a scenario in which partial alteration of the wall rock caused the release of Al and K from primary feldspars that precipitated kaolinite and I-S locally. Reactions of hydrothermal fluid with the parent andesite would have increased the pH high enough to stabilize carbonate precipitates as a late phase (Keith and Bargar, 1988; Bargar and Keith, 1999). The overall mineralogy, in particular in the Sulfur mine region and the presence of elemental sulfur are characteristic of intermediate argillic zones with high-sulfidation epithermal alteration at temperatures below 300°C (Hedenquist and Lowenstern, 1994; Velde, 1995; Pirajno, 2009). The sharp transition from the interior parts of the vein [I-S, pyrite and sulfur] to exterior [carbonate, pyrite, plagioclase, smectite] suggests a short-lived alteration.

Samples from the Sulfur mine also show a sharp contrast in antibacterial activity (Fig. 11), with bactericidal samples found in the interior (hotter, acidic) parts of the vein where pyrite is abundant (up to 19%) and nonantibacterial samples found in the exterior cooler parts of the vein (Table 2), where samples contain less pyrite (<6 wt %) and the presence of carbonates

indicates an elevated pH. Significantly, the elemental sulfur was nonantibacterial against the *E. coli* and *S. epidermidis* tested.

Open Pit: Table 3 summarizes the mineralogy and antibacterial effect of representative samples from the Open Pit. Oxidized Red clay is located above the reduced Blue clay assemblage that dominates the Open Pit. The Red clay contains no detectible pyrite but rather goethite that most likely formed from the oxidation of pyrite. The Red clay assemblage is dominated by I-S, but also contains minor kaolinite and chlorite, which may have formed under more acidic conditions generated by pyrite oxidation. The Red clay is nonantibacterial.

The White clay (sample P2) contains 6.3 wt % smectite in addition to the rectorite. There is no detectible pyrite in this clay, yet the White clay is inhibitory to bacterial growth. Secondary minerals gypsum and jarosite are present in this zone and are characteristic of acidic mine environments as a result of pyrite oxidation (Murad and Rojik, 2003, 2005).

Blue clay in the Open Pit is the most abundant alteration type and is consistently bactericidal. The mineralogy of the Open Pit Blue clays is dominated by rectorite (55% I, R1-ordered I-S, in the field identified as pyrophyllite) together with abundant quartz, illite, and pyrite (Table 3), suggesting acid-sulfate alteration water (White and Hedenquist, 1995).

A stockwork of randomly oriented veins containing abundant quartz and pyrite are present in the Blue clay alteration (Fig. 12). Quartz veins are typical of the low- to intermediate-sulfidation environment formed at temperatures <300°C and depths <3 km (Hedenquist and Lowenstern, 1994). The Open Pit Blue clay may have formed by a pervasive low-temperature (150°–200°C) low-sulfidation fluid, with periods of rapidly ascending SiO₂-rich fluids from depth-filling fractures with quartz. The relatively high proportion (>9 wt %) of crystalline pyrite (>20 μm) in these quartz veins contrasts with the submicron pyrite (4–6 wt %) that dominates the Blue clay. Interestingly however, samples of the stockwork are nonantibacterial, despite the high amount of pyrite, which suggests pyrite particle size and clay mineral content are important variables in the antibacterial reaction.

The Blue clay in the Open Pit was sampled at the interface with the Red clay down to 1.5 m at 0.3-m intervals. The Blue clay sampled just below the oxidized zone (0.1-m depth) contains pyrite and jarosite (Fig. 12; Table 3, sample P3) and

Table 2. Sulfur Mine XRD (results are reported as mineral wt %)

Sample	Antibacterial activity	Quartz	Plagioclase	Calcite	Dolomite	Pyrite	Sulfur	Gypsum	Jarosite	Kaolinite	Smectite	I-S >70%
S1	-	37.5			5.5	4.6		0.6	0.4	5.1		41.9
S2	-	42.8		1		5.9				4.4		46.9
S3	++	38.1				8.3			1.5	3.1	9.3	36
S4	++	34.9				18.7	5.2					37.5
S5	++	35.8				13.3			1.3			49.6
S6	++	28.9				5.5				1.4	45.7	17.8
S7	++	13.5				10.8	50.4					22.7
S8	++	39.5				11.5	1.7		2.2	3.1		41.3
S9	-	18.1	21.6	2.7		5.1		2.7			46.8	
S10	-	19.9	31.9			1.2		2.9			43.3	

Notes: Antibacterial activity for *E. coli* and *S. epidermidis* expressed as bactericidal (++), growth inhibition (+) or nonantibacterial (-); I-S = illite-smectite

Table 3. Open Pit XRD (quantitative XRD results reported as mineral wt %)

Sample	Depth	Antibacterial activity	Quartz	Plagioclase	Pyrite	Gypsum	Jarosite	Goethite	Rectorite	Chlorite	Smectite	Kaolinite
P1	0.0 m	-	36.3	4.6				3.4	44.6	3.5		4.7
P2	0.0 m	+	48.5	2.9		2.7			36.6		6.3	
P3	0.1 m	++	46.5		4.6	1.1	1		42			
P4	0.1 m	++	45.3	0.8	4.4	0.8	0.7		48.3			
P5	0.3 m	+	45.8	0.6	4.6	0.4	1.2		42.1			
P6	0.6 m	+	42.9		4.6	1.2	0.9		45.3			
P7	0.6 m	+	42.3	0.4	4.3	1.2			46.6			
P8	0.9 m	+	42.2		5	1.9			47.4			
P9	0.9 m	+	42.6		5.4	2.1			46.1			
P10	1.2 m	+	43.7	0.7	5	1.9			49.1			
P11	1.2 m	+	42.6		5.6	1.6			46.7			
P12	1.5 m	-	41.9		6.5	2.4			48.1			
P13	Stock work	-	70.2		9.4				19.7			
P14	Fault	+	32.8						65.7			

Surface samples are from the oxidized red (P1) and white (P2) zones

Blue clay samples were taken at the interface of the oxidized zone from 0.1–1.5 m depth; antibacterial activity for *E. coli* and *S. epidermidis* expressed as bactericidal (++), growth inhibition (+) or nonantibacterial (-)

is bactericidal. With increasing depth, jarosite disappears as the oxidation state decreases with depth and the Blue clay becomes less bactericidal, only inhibiting bacterial growth. Pyrite concentrations in the Blue clay are fairly uniform (4–6 wt %), however the oxidation state of the Blue clay equilibrated with DIW shows a decrease with depth, suggesting an important role of Eh in the antibacterial reactions.

Geochemical trends for rehydrated clays from surface to depth in the Open Pit (Fig. 13) show increasing antibacterial effectiveness with increasing Eh and aqueous metal content, which is linked to hydrogen peroxide (H_2O_2) production (Fig. 13A-D). Pyrite wt % decreases near the surface due to

oxidation, which together with metal hydrolysis results in a decrease in pH near the surface (Fig. 13E-F).

Foster Creek: The Blue clay assemblage sampled in the Foster Creek drainage contains calcite, dolomite, smectite, kaolinite, and pyrite (Table 4). Carbonates most likely precipitated as temperature decreased and fluid pH increased by leaching Ca and Mg from the parent rock. The late precipitation of carbonates has been observed in similar hydrothermal systems (Keith and Bargar, 1988; Bargar and Keith, 1999). Pyrite concentrations were generally 4 to 5 wt % throughout the Foster Creek Blue clay alteration. Samples F1 to F4 (Table 4) contain plagioclase (7–21 wt %), smectite (up to 49 wt %),

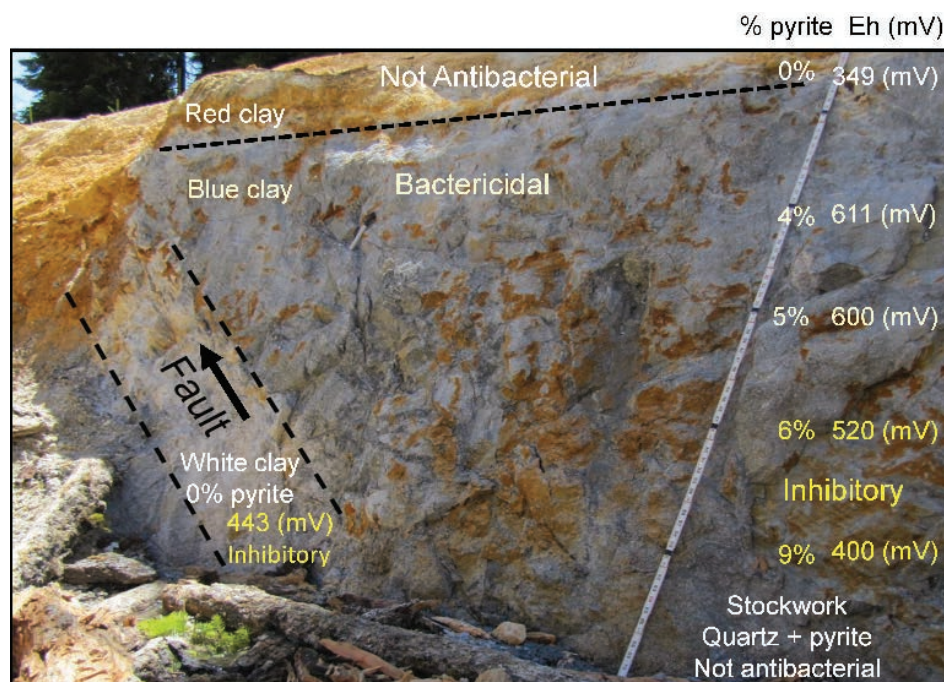


Fig. 12. Cross section through the Open pit. (Top) Red surficial clay, (Bottom left) White clay in fault zone, and (Middle) massive Blue alteration assemblages sampled over 1.5-m depth. A stockwork of rusty quartz-pyrite veins is disseminated in the Blue clay (ruler black markers indicate 0.3-m intervals).

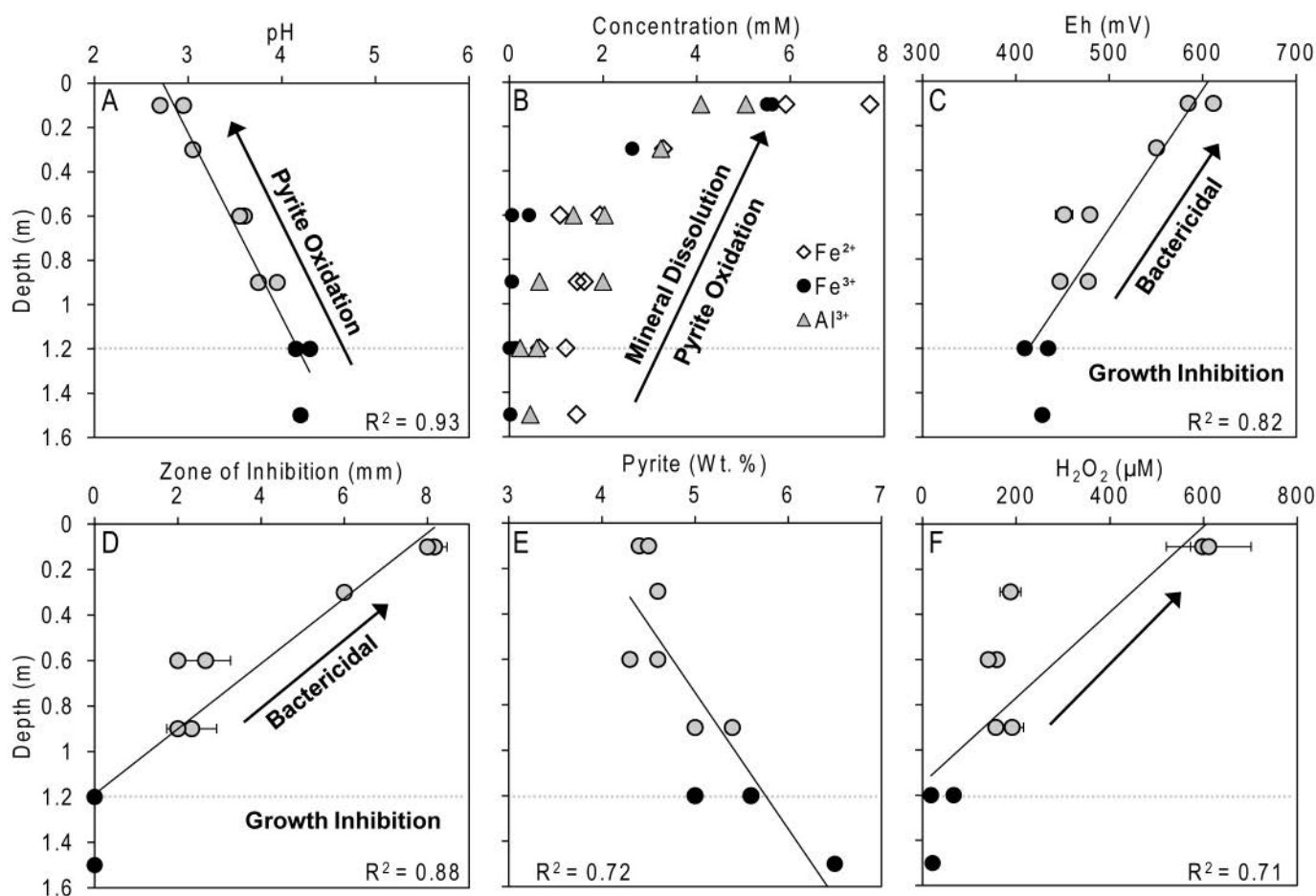


Fig. 13. Geochemical trends with depth in the Open Pit. Samples of Blue clay from 0.1- to 1.5-m depth show (A) increasing antibacterial effectiveness near surface, following (B) increasing Eh, (C) increasing dissolved Fe, Al content (D) increasing hydrogen peroxide production. Oxidation and hydrolysis reactions cause reduced pyrite content and lower pH near surface. Dotted line marks the depth where samples transition from bactericidal (gray dots) to inhibitory (black dots).

Table 4. Quantitative XRD for Foster Creek and Road Cut Sampling Sites (results are reported as mineral wt %)

Location	Sample	Antibacterial activity	Quartz	Plagioclase	Calcite	Dolomite	Pyrite	Gypsum	Jarosite	Kaolinite	Smectite	I-S >70%
Foster Creek	F1	-	31	7.3	4.3		4.3			1.9	21.3	26.9
	F2	-	36.7	20.7	1		3.7			1.5	12.5	24.8
	F3	-	33.5	6.7	3.6		4.8			3.5	41.9	
	F4	-	21.4	9.8	10.8		0.8			7.5	48.9	
	F5	-	30.4	0.5		17.3	3.4	1.7		5.5		38.8
	F6	-	39	2.8		2.4	5.5	1.9		3.7		44.9
	F7	-	38.1			3.2	6.2	2.9				46.9
	F8	++	40.5				4.7	1.8	1.1			49.3
	F9	++	42.3				4.3	1.1				46.6
Road Cut	C1	-	40.6	19.5						3.4		29.3
	C2	-	44.6		11.3		0.4			16.8		24.1
	C3	-	36.5		5.7		3	1.6		6.3		45.3
	C4	+	38.1				4.8	1.5				49.8
	C5	-	47.2		3.2		1	0.3		17.4		29.6
	C6	-	45		8.9					13.4		28.1
	C7	-	45.6		9.7					12.8		27.9
	C8	-	54.3		3		1.2			8		33.5
	C9	-	50.7				1.3			13.3		30.8

Notes: Antibacterial activity for *E. coli* and *S. epidermidis* expressed as bactericidal (++), growth inhibition (+) or nonantibacterial (-)

kaolinite (up to 8 wt %), and calcite (up to 11 wt %), indicating incomplete alteration of the parent andesite (Reyes, 1990). Samples F5 to F7 (Table 4) contain up to 17 wt % dolomite but are dominated by 39 to 47 wt % I-S (70% illite; $R > 1$), with minor kaolinite (<6 wt %) and plagioclase (<3 wt %). The absence of smectite from the mineral assemblage is consistent with a higher temperature of alteration indicated by the 70% illite in I-S. The only bactericidal samples found at this location were samples F8 and F9 that are dominated by I-S (47–49 wt %), quartz (~40–42 wt %), and pyrite (4–5 wt %). The appearance of jarosite indicates a relatively high oxidation state in the environment of the antibacterial samples (Brown, 1971), as observed in near-surface samples from the Open pit. The absence of carbonates in these antibacterial samples (Table 4), suggests a low pH environment where carbonates are not stable.

Road Cut: Blue clay alteration around a 10-m-wide fault zone was identified in the Road Cut (FS6520), southwest of Foster Creek. A cross section of the zone was sampled over ~5 m, to gauge the mineral alteration from the parent rock toward the central fault plane. The alteration minerals present in this zone are quartz (37–54 wt %), I-S (85% illite; R3

ordered), ranging from 34 to 57 wt %, kaolinite (<17 wt %) and minor calcite, pyrite, and gypsum (Table 4). Only the altered wall rock contained plagioclase feldspar (~20 wt %), reflecting incomplete alteration of the andesite. Sample C4 inhibited bacterial growth and, significantly, this sample does not contain calcite or kaolinite, but contains the highest concentration of pyrite (~5 wt %) in the cross section. No antibacterial activity was observed in samples containing calcite where $\text{pH} > 5$ reduces metal solubility of aqueous chloride and sulfate complexes (Migdisov and Williams-Jones, 2014).

Antibacterial correlations with geochemistry

Geochemical trends in antibacterial effectiveness of the OMT clays were used to deduce controls on the antibacterial reactions (Fig. 14). Antibacterial activity, determined by disk diffusion zones of inhibition and plate-counting methods, allowed a survey of representative samples from each alteration zone identified in the field. The antibacterial susceptibility was measured on both *E. coli* (ATCC 25922) and *S. epidermidis* (ATCC 14990) and is linked to solutions pH and Eh, which are controlled by the mineral assemblage when DIW is added to rehydrate the clay for medicinal application. Antibacterial

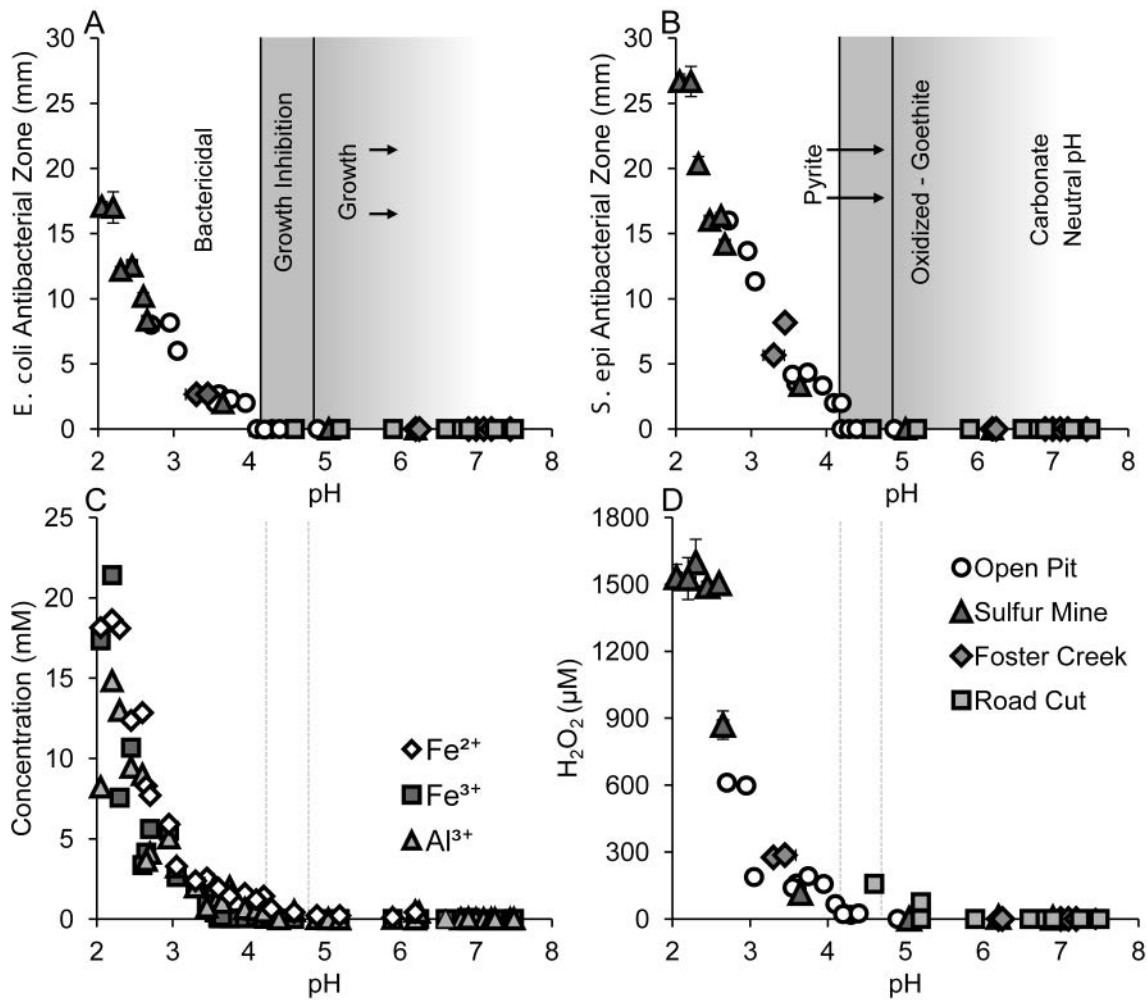


Fig. 14. Disk diffusion antibacterial susceptibility results of (A) *E. coli* and (B) *S. epidermidis* as a function of pH. The shaded areas correspond to antibacterial effectiveness. (C). Aqueous metal, and (D) hydrogen peroxide concentrations vs. pH. The dashed lines (C, D) correspond to the shaded antibacterial effectiveness regions in (A) and (B).

susceptibility testing against antibiotic resistant strains of model bacteria (*E. coli* ATCC 35218 and *S. epidermidis* ATCC 35948) produced similar results.

During oxidation of pyrite in the clay, reactive oxygen species (ROS) are produced, including hydrogen peroxide (H_2O_2) and radical species (Schoonen et al., 2010), following the well-known Fenton reaction series (Fenton, 1894). Either dissolved O_2 or Fe^{3+} can oxidize Fe^{2+} in pyrite when hydrated (Rimstidt and Vaughn, 2003). Hydroxyl radicals react within nanoseconds with biomolecules and are known to degrade organics (Repine et al., 1981; Imlay et al., 1988). However, due to the short existence of radical species the more stable coproduct of Fenton reactions, H_2O_2 , is commonly measured as an indicator of the radical production (Cohen et al., 2006).

The zones of inhibition for the gram-negative *E. coli* and gram-positive *S. epidermidis* both decrease with increasing pH (Fig. 14A-B). Simultaneously, the concentrations of the major metal species in solution (Al , Fe^{2+} , Fe^{3+}) decrease and hydrogen peroxide concentrations decrease. Bactericidal samples all have pH values <4.2 , with dissolved Fe^{2+} , Fe^{3+} , and Al^{3+} concentrations over 1 mM. The most antibacterial samples are from the Sulfur mine location, which contains elevated pyrite (10–18%), I-S (70–75% illite; $R > 1$), and jarosite, producing zones of inhibition >17 mm. The Open Pit Blue clays contain less pyrite (4–6 wt %) and show smaller zones

of inhibition. Samples from the White clay zones inhibited bacterial growth when tested by plate counting but did not produce a significant zone of inhibition in the disk diffusion test. These samples released lower concentrations of metals (<1 mM) with pH values ranging from 4.2 to 4.7. Bacterial growth is not affected in samples with $pH >4.7$, where hydrogen peroxide production becomes negligible (Fig. 14D).

Trends in the antibacterial effect show increasing zones of inhibition with increasing pyrite wt % (Fig. 15A). The crystal size of pyrite can affect oxidation and dissolution, due to greater reaction rates for the smaller size fractions (Schoonen et al., 2010). The small crystal size provides greater surface area for pyrite oxidation, increasing Fe solubility, and H_2O_2 generation. Black clay from the Sulfur mine contained very fine ($<1 \mu m$) disseminated pyrite that can rapidly oxidize when DIW is added. The Open Pit Blue clays may form smaller zones of inhibition because much of the pyrite is in the form of large ($>20 \mu m$) crystals, but the more reactive pyrite is submicron size (Williams et al., 2004). Hydrogen peroxide production decreases with increasing pH and parallels the pyrite concentration (Fig. 15B-C). Significantly, carbonate becomes stable as the pH increases above 5, due to the interaction of hydrothermal fluids with the parent rock (Fig. 15D).

The most effective antibacterial samples were the Sulfur mine Black clays and the Open Pit Blue clays. Table 5

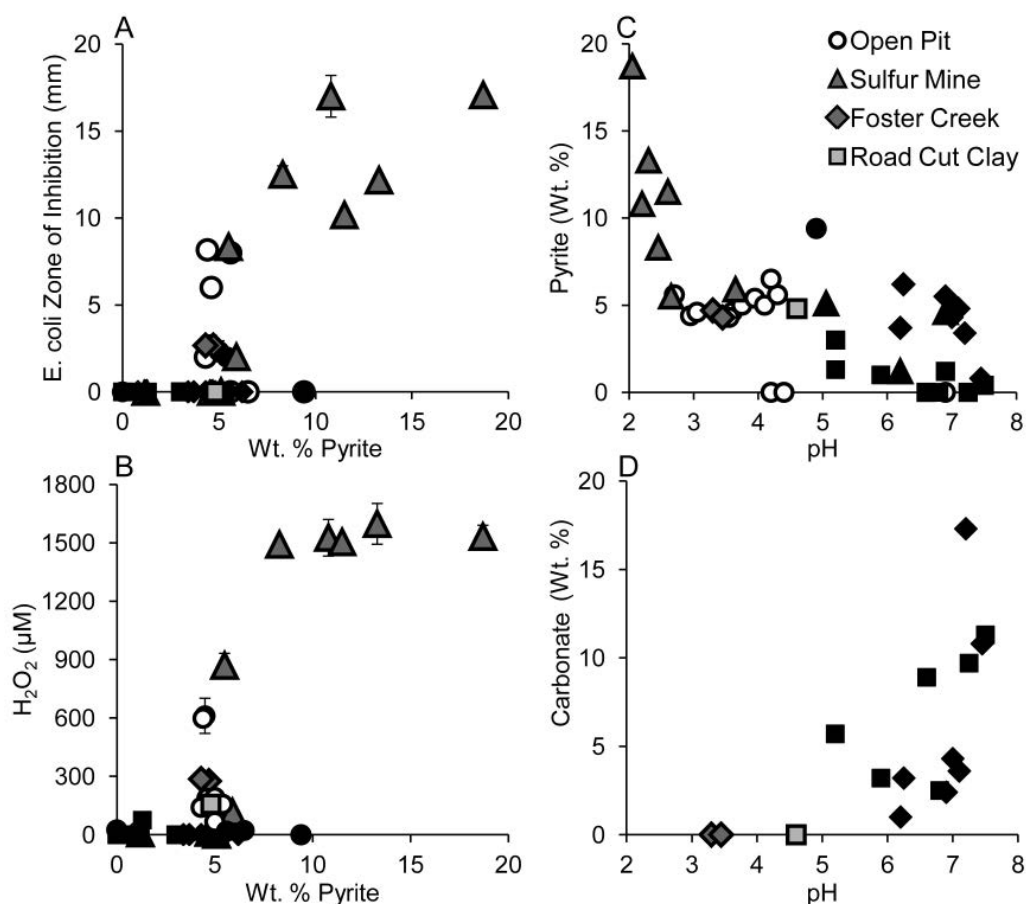


Fig. 15. Trends in pyrite and carbonate compared to antibacterial effectiveness indicated by growth inhibition. (A). *E. coli* zone of inhibition (mm). (B). Hydrogen peroxide concentration vs. pyrite wt %. (C). Trend in pyrite wt %. (D). Carbonate wt % with pH of the hydrated mineral suspensions.

Table 5. Comparison of the Aqueous Leachate Chemistry (μM) of Representative Samples Measured by ICP-MS

Element	Open Pit		Sulfur mine			Foster Creek		Road Cut	
	Blue (P4)	White (P2)	Red (P1)	Black(S4)	Blue (S6)	Blue (F8)	Blue (F1)	Blue (C4)	Blue (C3)
Na	34.2	39.1	43.4	239.9	193.3	62.8	190.2	53	435.6
Mg	749.2	274.3	13.8	660.1	1,114.1	2,509.3	155.2	497.5	384.2
Al	4,599.80	456.3	54.4	8,208	3,646.9	2,065.5	1.4	62.9	38.2
P	233.3	1.7	1.2	96.1	19.5	24.1	5.8	0.7	0.3
K	0.7	44.2	11.8	198.2	65.2	1.8	96	374.7	424.4
Ca	3,933.70	11,176.1	35.8	523.1	1,734.50	4,612	1,176.20	4,775.40	4,209.70
Ti	0.2	0.28	2.81E-02	0.3	0.1	0.1	6.10E-03	2.00E-02	4.40E-03
V	1.3	4.73E-03	2.67E-02	7.8	16.8	0.2	7.60E-03	BDL	BDL
Cr	0.8	0.12	1.15E-02	5.5	4.4	0.1	5.90E-03	3.00E-03	1.70E-03
Mn	30	11.8	0.19	120.2	239.7	71.3	2	12.8	14.5
Fe ²⁺	5,885.20	224.8	0	18,137.5	8,283.9	2,374.9	30.4	422.8	101.9
Fe ³⁺	5,456.30	504.2	11.9	17,134.2	4136	2,010.5	BDL	13.5	7.8
Co	6.5	0.4	2.75E-03	21.2	7.5	4.3	1.10E-02	3.4	2.7
Ni	8.3	0.38	8.67E-03	30.1	13.1	4.8	0.1	1	0.8
Cu	11.8	1.9	4.27E-02	35.2	13	6.1	0.2	0.7	0.6
Zn	5.8	2.8	9.57E-02	36.7	31.6	4.6	1.9	5.3	3.8
As	1.4	BDL	BDL	1.9	0.2	0.1	BDL	1.20E-01	0.2
Se	0.8	4.40E-02	BDL	0.9	0.5	0.6	7.80E-03	2.90E-02	2.50E-02
Rb	3.80E-02	6.40E-02	5.85E-03	0.2	3.70E-02	9.80E-03	8.70E-03	9.40E-02	8.90E-02
Sr	18	7.9	0.15	6.2	12.3	7.7	3.3	32.2	35.9
Mo	0.1	2.60E-02	2.49E-03	0.1	3.20E-02	9.60E-03	1.30E-02	4.10E-03	2.90E-03
Cd	8.00E-03	1.60E-03	BDL	0.2	0.4	9.50E-03	2.20E-03	9.60E-03	1.00E-02
Cs	2.10E-02	5.80E-03	2.34E-03	---	---	7.00E-03	3.00E-03	1.00E-03	BDL
Ba	1.60E-02	1.10E-01	1.34E-02	0.4	0.1	0.1	0.4	0.5	0.5
Hf	BDL	BDL	BDL	BDL	BDL	BDL	BDL	BDL	BDL
W	1.60E-03	BDL	BDL	1.60E-03	---	1.60E-03	BDL	4.30E-03	8.30E-02
Ag	BDL	BDL	BDL	---	---	BDL	BDL	BDL	BDL
Hg	BDL	BDL	BDL	---	---	BDL	BDL	BDL	3.10E-03
Pb	BDL	BDL	BDL	---	---	0.4	3.00E-02	0.2	0.1
U	2.30E-03	BDL	BDL	---	---	4.10E-03	BDL	3.80E-03	2.90E-03
pH	2.9 \pm 0.1	4.2 \pm 0	6.8 \pm 0	2.0 \pm 0.1	2.7 \pm 0.1	3.3 \pm 0.1	7.0 \pm 0	4.2 \pm 0.1	5.3 \pm 0.1
Eh (mV)	611 \pm 1.3	443 \pm 1.5	349 \pm 10.1	724 \pm 0.4	594 \pm 15.0	520 \pm 3.3	368 \pm 1.6	408 \pm 6.7	367 \pm 2.1

Notes: Relative standard deviations for elemental analysis were <7.0%; nonantibacterial samples shaded gray
BDL = below detection limit; --- = not measured

compares the solution chemistry of representative samples of the clay collected from these sample locations. Samples from the Sulfur mine generate the highest amounts of Fe and Al, producing a very low pH (<2.7). Black clay (Table 2, Sample S4), containing up to 19 wt % pyrite, produced the highest aqueous metal content and lowest pH (2.0). Samples with lower pyrite concentrations (~5 wt %) produce lower amounts of Fe and Al at slightly higher pH (2.7). Bactericidal samples from the Open Pit Blue clay have pH <4.2 and contain >1-mM concentrations of Fe²⁺, Fe³⁺, and Al³⁺ and Ca. The White clay (Table 1, sample P2) contained no measurable pyrite but still released significant Fe and Al (Table 5). Bactericidal samples from Foster Creek (Table 4; samples F8, F9) contained ~ 4 wt % pyrite and released ~2-mM Fe²⁺, Fe³⁺, and Al³⁺ at a pH of 3.3. For the Road Cut, only one sample (Table 4; sample C4) inhibited bacterial growth at pH 4.2. The major anion in the OMT leachates is sulfate (>2,000 $\mu\text{g}/\text{ml}$) with <7 $\mu\text{g}/\text{ml}$ phosphate and <1 $\mu\text{g}/\text{ml}$ chloride (Williams et al., 2011).

Nonantibacterial samples have pH >5, and Eh values below 400 mV. Samples collected from the Foster Creek and Road Cut sites that contain carbonates show no antibacterial effect. The solution chemistry of aqueous leachates of these samples (Table 5) shows very low levels of soluble Fe and Al compared

to the antibacterial samples. These results all indicate that the pH and Eh, and the solubility and toxicity of the metals leached from the OMT clays are linked to their antibacterial activity (Morrison et al., 2016).

Carbonates were present in the majority of the samples from the Foster Creek and Road Cut sites, which eliminated their antibacterial activity (Table 4) due to increases in pH (Fig. 16) to where Fe²⁺ is not stable. The elements leached from antibacterial and nonantibacterial samples from these sites are compared in Table 5. Bactericidal samples from Foster Creek (samples F8, F9) contained ~4 wt % pyrite and produced ~2 mM Fe²⁺, Fe³⁺, and Al³⁺ at low pH (3.3). The nonantibacterial clays from Foster Creek, containing carbonate, had near-neutral pH, and released only μM concentrations of Fe and Al (Table 5). The same trend is observed in the Road Cut, where only sample C4 inhibited bacterial growth (pH 4.2).

Aqueous metal speciation changes under varying pH and Eh conditions; therefore modeling of the aqueous species sheds light on the antibacterial process. Figure 16 shows pH and Eh values of mineral suspensions (100 mg clay/ml in 10 g LB/ml) in stability diagrams calculated for Fe and Al in an S-rich fluid. When samples are mixed with bacteria in growth media (LB), the pH and Eh of the system shift toward more oxidized, higher pH conditions, and eventually goethite

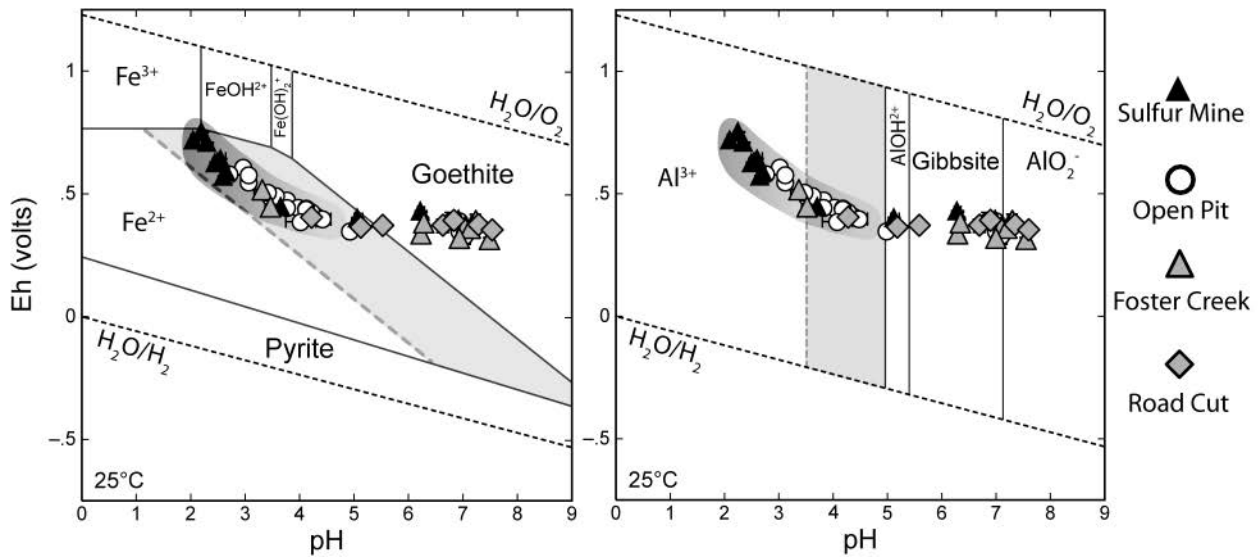


Fig. 16. Eh-pH plots showing (A) Fe-S-O-H and (B) Al-S-O-H systems at 25°C. Shaded areas represent aqueous Fe^{2+} and Al^{3+} at concentrations measured in OMT leachates (100 mg/ml clay), and indicate the stability change approaching equilibrium. Circled samples (dark gray) are antibacterial.

precipitates. As discussed above, the bactericidal samples have pH values <4.5 and Eh >400 mV, where >1-mM concentrations of aqueous Fe^{2+} , Fe^{3+} , and Al^{3+} are released during mineral dissolution.

Discussion

Our goal in studying the detailed geologic field relationships of the OMT argillic alteration was to identify the important mineralogical variables that affect the antibacterial properties of clays. Although this deposit is just one of the antibacterial clays that has been identified worldwide (Williams and Haydel, 2010; Londoño et al., 2017), it represents mineralogical characteristics of other antibacterial clays and contains the most effective antibacterial clay we have found in over a decade of testing. By identifying the geologic environments that form such deposits, we may find others like it, providing new economic value to a previously unrecognized resource.

The antibacterial clays identified in the OMT deposit formed from acidic-sulfur rich waters that produced intermediate argillic clay zones containing predominantly illite-smectite (I-S), pyrite, and quartz, with minor plagioclase, chlorite, kaolinite, and accessories. The antibacterial activity depends on the pH and Eh of the clays rehydrated with DIW at a concentration (100 mg/ml) that promotes mineral dissolution, oxidation, and the release of soluble metals that drive the reactions responsible for killing a broad spectrum of human pathogens. Iron (Fe^{2+}) and Al^{3+} are the soluble metals responsible for the bactericide in this deposit, through a synergistic attack of the cell wall and intracellular proteins by oxidation and production of hydroxyl radicals (Morrison et al., 2016).

The precipitation of elemental sulfur in the Sulfur mine indicates a high-sulfidation epithermal alteration (Hedenquist and Lowenstern, 1994). The mineral assemblage (sulfur, pyrite, I-S, kaolinite, and smectite) indicates intermediate argillic alteration from high-sulfidation fluids. The S-rich fluid needed to produce the high sulfide content would

disproportion into sulfuric acid and H_2S (g) at elevated temperatures (250°–280°C) as it ascended through rock fractures under reducing conditions (White and Hedenquist, 1995; Delmelle et al., 2000; Pirajno, 2009). The precipitation of sulfur may have occurred at temperatures as high as 200°C at depth (Susse et al., 1966; Barnes, 1997; Bons, 2001; Pirajno, 2009; Naumov et al., 2015) or near surface at temperatures as low as 119°C (Barnes, 1997). The large sulfur crystals reflect a late-phase cooling of hydrothermal fluids in this region.

The formation of I-S due to hydrothermal alteration can take place in a geologically short time span (10–10,000 yr), depending on the temperature and fluid chemistry (Meunier, 2005). The formation of R1-ordered I-S is estimated to occur in as little as 10 years if temperatures are >250°C, whereas at 150°C this process may require on the order of 10,000 years (Meunier, 2005). The more highly illitic (up to 85% illite in I-S) clays observed in the Sulfur mine, Foster Creek, and Road Cut sample sites are associated with fractures and faulting and may have formed rapidly at relatively high temperature (~300°C). However, the Open Pit exposes more massive clay (meters thick) dominated by rectorite with minor pyrite and most likely formed from more diffuse and pervasive hydrothermal waters.

The oxygen isotope measurements of secondary quartz from these different sample sites were interpreted using the mineralogical estimates of temperature to indicate fluid sources. Secondary quartz associated with pyrite-rich Black clay from the Sulfur mine has the highest $\delta^{18}\text{O}$ values (20–25‰) in clay dominated by I >70 % illite in I-S (Table 2; samples S4, S5). The absence of end-member illite, which is stable at 300°C at equilibrium, suggests that temperatures must have been below this limit (Velde, 1995; Meunier, 2005). Furthermore, the R1 ordering of I-S indicates temperatures (depending on time) between 200° to 300°C (Velde and Lanson, 1993). The high $\delta^{18}\text{O}$ values (20–25‰) measured in quartz found in the Black clay may represent hydrothermal alteration of primary magmatic quartz, as described by King et al. (1997) for the

Kidd Creek deposit, Ontario, Canada. It is well known that oxygen isotope exchange occurs during hydrothermal alteration (Taylor and Huston, 1998; Tanner et al., 2015), driving $\delta^{18}\text{O}$ values higher (5–7‰) than the original magmatic composition. However, in the Black clay, the textures of the associated quartz indicate precipitation rather than replacement (Fig. 7). Thus, if the quartz formed at the maximum temperature (300°C) supported by I-S stability, then the water $\delta^{18}\text{O}$ composition in equilibrium with that clay was 10 to 15‰ (Fig. 8). The presence of large sulfur crystals in this zone indicates that as the system cooled, sulfur crystals grew at low pressures and temperatures as low as ~119°C. If the quartz precipitated at temperatures that low, the $\delta^{18}\text{O}$ of the water would have been considerably lighter (0–5‰), indicating possible mixing with meteoric water.

The antibacterial Blue clay in the Open Pit contains secondary quartz replacing plagioclase. The Blue clay is dominated by rectorite, so temperatures are estimated to have been as low as ~150°C (Pevear et al., 1980), consistent with a water $\delta^{18}\text{O}$ composition near 0‰. The White clay in the Open Pit formed along fault zones through the Blue clay and contains kaolinite and smectite, indicating that lower temperatures associated with meteoric water mixing. Using the published range of meteoric water compositions determined for the Cascades over the last 30 Ma (–5 to –15‰; Kohn et al., 2002), one can determine the quartz precipitation temperatures of the White clay. From these meteoric water values and measured quartz $\delta^{18}\text{O}$ values (+1 to +8‰) equilibrium temperatures of 100° to 200°C are required, which agrees with the mineralogical indications of lower temperature.

The Blue antibacterial clays (rectorite, pyrite, and quartz) formed under low-sulfidation alteration, and they are bactericidal when the pH and Eh of the clay suspensions are <4.2 and >400 mV, respectively. It is notable that the most bactericidal samples are found near the surface of the Open Pit where Eh is highest. These samples released 5 to 10 mM Fe and Al, and generated up to 0.6 mM H_2O_2 . The antibacterial effect of the Blue clays decreased at greater depths (over 1.5 m), where the Eh decreased (Fig. 12), limiting the oxidation and mineral dissolution that could occur during the 24-hr equilibration with DIW. Samples at depth produced <1 mM Fe and Al and only inhibited bacterial growth. The complete oxidation of pyrite to goethite, as found in the surficial Red clays, eliminates the antibacterial effect. Goethite is stable at Eh >800, however when Red clays containing goethite are mixed with DIW, the electrical potential of the solution is <400 mV and pH increases to ~5 (Table 3; sample P1). Because Fe^{3+} precipitates under these conditions, these

samples only release μM concentrations of Fe rendering the Red clays nonantibacterial.

The Open Pit White clays, with no measureable pyrite, inhibit bacterial growth releasing lower (<0.5 mM) but significant amounts of Fe^{2+} , Fe^{3+} , and Al^{3+} (Table 5). The Fe and Al in solution may be derived from clay mineral dissolution and/or cation exchange. The average cation exchange capacity for the White clays is 23 ± 2 meq/100g, which is greater than other alteration zones (12–18 meq/100g) because of the presence of smectite. From the cation exchange capacity in the White clay, we calculate that up to 11.5 mM of divalent cations can be stored in the interlayer sites of the smectite, providing a potential reservoir for Fe^{2+} and Ca^{2+} released from mineral dissolution. Any pyrite or plagioclase originally present in the White clay fault zones infiltrated by meteoric water, probably dissolved, providing a source of these cations potentially adsorbed by the smectite.

Our study suggests that pH and Eh measurements of rehydrated clay samples in the field could provide a simple method to rapidly screen hydrothermal alteration zones for potential antibacterial activity. Samples can be collected, rehydrated (~100 mg clay/ml DIW), and measured directly in the field or dried (<60°C) and measured later in the lab. Clays that buffer fluids or generate oxidation reactions in the pH and Eh range where Fe^{2+} and/or Al^{3+} are soluble are candidates for being antibacterial. However, their effectiveness depends on the concentrations of the soluble metals (Al and reduced metals), and therefore those clays should be further tested by serial plate-counting methods (Clinical Laboratory Standards Institute (CLSI), 2015). Table 6 outlines the characteristics for identifying antibacterial clays based on the observed mineral assemblages, pH, and Eh measurements. These values are sensitive to the mineralogy and particle size (surface area) of the components, therefore the mineral/water ratio required for bactericide may vary. However, among the antibacterial clays we have studied, a concentration of 50- to 100-mg clay/ml DIW has proven antibacterial.

Conclusions

The OMT deposit formed from the hydrothermal alteration of volcanic rocks with basaltic to andesitic composition. The mineral assemblages that formed are characteristic of intermediate argillic alteration. The mineralogical assemblage in the Sulfur mine sample site indicated high-sulfidation. Acid-sulfate hydrothermal fluids most likely formed the pervasive Blue clay assemblage best exposed in the Open Pit. Intermediate-sulfidation fluids may be responsible for the clay alteration observed in the Foster Creek and Road Cut sample

Table 6. Characteristics of Antibacterial Clay Zones in Hydrothermal Deposits

Antibacterial activity	Alteration type	Mineral assemblage	pH	Eh (mV)
Bactericidal	High, low-sulfidation	Pyrite (>4%), Illite-smectite, quartz	<4.2	>600
Growth inhibition	Low-sulfidation	Pyrite (4–6%), Illite-smectite, quartz	4.2–4.7	>400
Growth inhibition	Low-sulfidation, bleached zone	Illite-smectite, quartz	4.2–4.7	>400
Nonantibacterial	Low, high-sulfidation, carbonate-rich or red oxidized surface	Illite-smectite, pyrite, carbonate, goethite (all pyrite oxidized)	5–7	<400

Notes: Mineral samples were rehydrated with deionized water using a 100 mg/ml mineral/DIW ratio equilibrated by shaking for 24 h; ore concentrated suspensions may be required

locations, based on the mineralogy and indicated higher temperatures of emplacement.

The pervasive nature of rectorite in the Open Pit and secondary quartz $\delta^{18}\text{O}$ values suggest a constant heat source (150°–200°C) with mixing of magmatic and meteoric waters. The other clay zones sampled contain I-S with higher % illite layers (70–80%), pyrite, and in some samples kaolinite and carbonate. The more acidic fluids associated with intermediate- to high-sulfidation alteration promote Al solubility and kaolinite formation. The alteration in these zones was most likely a short-lived event compared to the hydrothermal activity in the Open Pit. Relatively rapid alteration in faults and fractures is indicated by the presence of carbonates, which require pH neutralization from Ca and Mg dissolution of the parent rock. Carbonates therefore represent a late-phase mineralization as fluids cooled, after the initial high-temperature acidic alteration.

Antibacterial susceptibility testing indicates that the presence of pyrite alone does not prescribe bactericide but rather that the oxidation state of the pyrite-bearing clays and the pH buffered by the clay assemblage controls the bactericidal reactions. Clays formed in the high-sulfidation environment documented in the Sulfur mine site are the most antibacterial. The high pyrite content (~19%) and small crystal size (<1 μm) in this zone promotes oxidation and mineral dissolution, releasing Fe^{2+} , Fe^{3+} , and Al^{3+} (>10 mM) while generating hydrogen peroxide (H_2O_2 >500 μM), indicating hydroxyl radical production which leads to bactericide (Morrison et al., 2016).

Samples from the Open Pit Blue clay have lower pyrite concentrations (4–6 wt %) and are bactericidal when pH and Eh conditions promote mineral dissolution, metal oxidation, and H_2O_2 generation. The Blue clay shows decreasing antibacterial effectiveness with depth due to the decreasing Eh of the mineral assemblage. The most bactericidal samples were found at the interface with more oxidized samples near the surface. Jarosite appears in the bactericidal samples of Blue clay, suggesting that oxidizing conditions (Eh 600–750 mV) are required for bactericide. The Open Pit White clays located along faults contained no iron sulfides but still inhibit bacterial growth through the release of Fe^{2+} and Al^{3+} at pH 4.7, and Eh as low as 400mV. The White clays may release Fe^{2+} from exchange sites in smectite interlayers, when dilute DIW disrupts the geochemical equilibrium, driving exchange cations into solution. The Red oxidized zone in the Open Pit contains goethite from the oxidation of pyrite and is not antibacterial. Where goethite is stable the oxidation state is too high for aqueous Fe^{2+} stability. Samples containing carbonates showed no antibacterial activity, most likely due to increases in pH that stabilize the carbonates, but lower pyrite oxidation rates and metal hydrolysis.

The results from this study represent the first attempt to identify the hydrothermal processes that generate antibacterial clay deposits, opening the potential for a new economic geology and use for argillite alteration zones that are often considered to be overburden during ore exploration. These data show that there is not a simple relationship between alteration mineralogy and antibacterial activity. The antibacterial activity of the clays taken from their geologic environment is influenced by changes in the pH and Eh when DIW is added

to the mineral assemblage, changing the mineral equilibrium and driving oxidation and metal hydrolysis. The variations in antibacterial activity of different clay alteration zones documented in the OMT deposit can be used to predict where to find other antibacterial clay resources. Using the mineralogical and geochemical parameters that define the solubility of Fe^{2+} (or other redox sensitive metals) one can evaluate potential antibacterial clay deposits worldwide.

Acknowledgments

This research was supported by National Science Foundation grant EAR-1123931. The National SIMS Facility at ASU is supported by NSF grant EAR-1352996. We are grateful to R. Misra for advising the microbiology; ICP-MS was conducted in the Keck Environmental Laboratory with assistance from Steve Romaniello. We thank Oregon Mineral Technologies for access to their clay deposit and for field support, and Dennis Eberl (USGS, Boulder) for supporting X-ray diffraction and for valuable discussions.

REFERENCES

- Anastácio, A.S., Harris, B., Yoo, H., Fabris, J.D., and Stucki, J.W., 2008, Limitations of the ferrozine method for quantitative assay of mineral systems for ferrous and total iron: *Geochimica et Cosmochimica Acta*, v. 72, p. 5001–5008.
- Bacon, C.R., 2008, Geologic map of Mount Mazama and Crater Lake caldera, Oregon: U.S. Geological Survey Scientific Investigations Map 2832, version 1, p. 1–47.
- Baedecker, P.A., 1987, Methods for geochemical analysis: U.S. Geological Survey Bulletin 1770, 187 p.
- Baertschi, P., 1976, Absolute ^{18}O content of standard mean ocean water: *Earth and Planetary Science Letters*, v. 31, p. 341–344.
- Bargar, K.E., and Keith, T.E., 1999, Hydrothermal mineralogy of core from geothermal drill holes at Newberry volcano, Oregon: U.S. Geological Survey Professional Paper 1578, p. 7071–7076.
- Barnes, H.L., 1997, *Geochemistry of hydrothermal ore deposits*: New York, John Wiley and Sons, 972 p.
- Bauer, A.W., Kirby, W.M.M., Sherris, J.C., and Turck, M., 1966, Antibiotic susceptibility testing by a standardized single disk method: *American Journal of Clinical Pathology*, v. 45, p. 493–496.
- Beaty, D.W., and Hugh, P.T., 1988, An oxygen isotope study of the Kidd Creek, Ontario, volcanogenic massive sulfide deposit: Evidence for a high ^{18}O ore fluid: *Economic Geology*, v. 83, p. 1–17.
- Bindeman, H., 2008, Oxygen isotopes in mantle and crustal magmas as revealed by single crystal analysis: *Reviews in Mineralogy and Geochemistry*, v. 69, p. 445–478.
- Bons, P.D., 2001, The formation of large quartz veins by rapid ascent of fluids in mobile hydrofractures: *Tectonophysics*, v. 336, p. 1–17.
- Brown, J.B., 1971, Jarosite-goethite stabilities at 25°C, 1 ATM: *Mineralium Deposita*, v. 6, p. 245–252.
- Brunet de Courrou, L., 2002, Study Group Report on Buruli Ulcer Treatment with Clay: WHO Advisory Group Meeting on Buruli Ulcer, 5th, Geneva, Switzerland, March 14–22, 2002, Report WHO/CDS/CPE/GBUI/2002.
- Carretaro, M.I., 2002, Clay minerals and their beneficial effects upon human health: A review: *Applied Clay Science*, v. 2, p. 155–163.
- Clayton, R.N., O'Neil, J.R., and Mayeda, T.K., 1972, Oxygen isotope exchange between quartz and water: *Journal of Geophysical Research*, v. 77, p. 3057–3067.
- Clinical Laboratory Standards Institute (CLSI), 2015, Methods for dilution antimicrobial susceptibility tests for bacteria that grow aerobically: Approved Standard, 10th ed., Wayne, PA, CLSI document M07-A10, v. 35, p. 1–45.
- Cohn, C.A., Pak, A., Strongin, D., and Schoonen, M.A.A., 2005, Quantifying hydrogen peroxide in iron containing solutions using leuco crystal violet: *Geochemical Transactions*, v. 6, p. 47–51.
- Delmelle, P., Bernard, A., Kusakabe, M., Fischer, T.P., and Takano, B., 2000, Geochemistry of the magmatic-hydrothermal system of Kawah Ijen volcano, East Java, Indonesia: *Journal of Volcanology and Geothermal Research*, v. 97, p. 31–53.

- Eberl, D.D., 2003, User's guide to rockjock: A program for determining quantitative mineralogy from powder X-ray diffraction data: U.S. Geological Survey Open-File report 03-78, 36 p.
- Einaudi, M.T., Hedenquist, J.W., and Inan, E.E., 2003, Sulfidation state of fluids in active and extinct hydrothermal systems: Transitions from porphyry to epithermal environments Society of Economic Geologists Special Publication 10, p. 285–314.
- EPA Method 200.8, 1999, Determination of trace metals in waters and wastes by inductively coupled plasma-mass spectrometry: Cincinnati, OH, United States Environmental Protection Agency, Revision 5.5, EPA-821R-99-017, 57 p.
- Faure, G., 1998, Principles and applications of geochemistry, 2nd ed.: New Jersey, Prentice-Hall, 626 p.
- Fenton, H.J.H., 1894, Oxidation of tartaric acid in presence of iron: Journal of Chemical Society Transactions, v. 65, p. 899–911.
- Ferrell, R.E., 2008, Medicinal clay and spiritual healing: Clays and Clay Minerals, v. 56, p. 751–760.
- Ferrero, T., 1992, Geologic mapping and sampling project, Foster Creek sulfur deposit: Ashland Oregon, Ferrero Geologic Consulting, Company Report, 40 p.
- Fiebelkorn, R.B., Walker, G.W., Macleod, N.S., McKee, E.H., and Smith, J.G., 1983, Index to K-Ar age determinations for the state of Oregon: Isochron/West, v. 37, p. 3–60.
- Giggenbach, W.F., 1997, Geothermal systems and mercury deposits, in Barnes, H.L., ed., Geochemistry of hydrothermal ore deposits: Wiley Publishing, p. 737–796.
- Hammond, P.E., 1979, A tectonic model for evolution of the Cascade Range: Pacific Coast Paleogeography Symposium 3, Los Angeles Society of Economic Paleontologists and Mineralogists, Pacific Section, p. 219–237.
- Haydel, S.E., Remenih, C.M., and Williams, L.B., 2008, Broad-spectrum in vitro antibacterial activities of clay minerals against antibiotic-susceptible and antibiotic-resistant bacterial pathogens: Journal of Antimicrobial Chemotherapy, v. 61, p. 353–361.
- Hedenquist, J.W., and Lowenstern, J.B., 1994, The role of magmas in the formation of hydrothermal ore deposits: Nature, v. 370, p. 519–527.
- Hedges, A.J., 2002, Estimating the precision of serial dilutions and viable bacterial counts: International Journal of Food Microbiology, v. 76, p. 207–214.
- Hervig, R.L., 1996, Analyses of geological materials for boron by secondary ion mass spectrometry: Reviews in Mineralogy, v. 33, p. 789–803.
- Hervig, R.L., Williams, P., Thomas, R.M., Schauer, S.N., and Stelle, I.M., 1992, Microanalysis of oxygen isotopes in insulators by secondary ion mass spectrometry: International Journal of Mass Spectrometry and Ion Processes, v. 120, p. 5–63.
- Hervig, R.L., Williams, L.B., Kirkland, I.K., and Longstaffe, F.J., 1995, Oxygen isotope microanalysis of diagenetic quartz: Possible low temperature occlusions of pores: Geochimica et Cosmochimica Acta, v. 59, p. 2537–2543.
- Hervig, R.L., Mazdab, F.K., Williams, P., Guan, Y., Huss, G.R., and Leshin, L.A., 2006, Useful ion yields for Cameca IMS 3f and 6f SIMS: Limits on quantitative analysis: Chemical Geology, v. 227, p. 83–99.
- Inlay, J.A., Chin, S.M., and Linn, S., 1988, Toxic DNA damage by hydrogen peroxide through the Fenton reaction in vivo and in vitro: Science, v. 240, p. 640–642.
- Jackson, M.L., 1979, Soil Chemical Analysis-Advanced Course, 2nd ed.: Madison, WI, Published by the author, 11th printing, 895 p.
- Keith, T.C., and Bargar, K.E., 1988, Petrology and hydrothermal mineralogy of the U.S. Geological Survey Newberry 2 drill core from Newberry caldera, Oregon: Journal of Geophysical Research, v. 93, p. 10174–10190.
- Kibanova, D., Nieto-Camacho, A., and Cervini-Silva, J., 2009, Lipid peroxidation induced by expandable clay minerals: Environmental Science and Technology, v. 43, p. 7550–7555.
- King, E.M., Barrie, C.T., and Valley, J.W., 1997, Hydrothermal alteration of oxygen isotope ratios in quartz phenocrysts, Kidd Creek mine, Ontario: Magmatic values are preserved in zircon: Geology, v. 25, p. 1079–1082.
- Kohn, M.J., Miselis, J.L., and Fremd, T.J., 2002, Oxygen isotope evidence for progressive uplift of the Cascade Range, Oregon: Earth and Planetary Science Letters, v. 204, p. 151–165.
- Komadel, P., and Stucki, J.W., 1988, Quantitative assay of minerals for Fe²⁺ and Fe³⁺ using 1,10-phenanthroline: III. A rapid photochemical method: Clays and Clay Minerals, v. 36, p. 379–381.
- Londoño, S.C., and Williams, L.B., 2016, Unraveling the antibacterial mode of action of a clay from the Colombian Amazon: Environmental Geochemistry and Health, v. 38, p. 363–379.
- Londoño, S.C., Hartnett, H.E., and Williams, L.B., 2017, The antibacterial activity of aluminum in clay from the Colombian Amazon: Environmental Science and Technology, doi: 10.1021/acs.est.6b04670, 8 p.
- McCarty, D., 2009, Sybilla Version 2.2.2, © Chevron Technology Company, a division of Chevron, U.S.A., Inc., San Ramon, CA, 16 p.
- Meunier, A., 2005, Clays: Berlin, Heidelberg, New York, Springer, 415 p.
- Miles, A.A., and Misra, S.S., 1938, The estimation of the bactericidal power of the blood: Journal of Hygiene, v. 38, p. 732–749.
- Migdisov, A.A., and Williams-Jones, A.E., 2014, Hydrothermal transport and deposition of the rare earth elements by fluorine-bearing aqueous liquids: Mineralium Deposita, v. 49, p. 987–997.
- Moore, D.M., and Reynolds, R.C., 1997, X-ray diffraction and the identification and analysis of clay minerals, 2nd ed.: New York, Oxford University Press, 378 p.
- Morrison, K.D., 2015, Unearthing the antibacterial activity of a natural clay deposit: Ph.D. dissertation, Tempe, Arizona, Arizona State University, 157 p.
- Morrison, K.D., Underwood, J.C., Metzge, D.W., Eberl, D.D., and Williams, L.B., 2014, Mineralogical variables that control the antibacterial effectiveness of a natural clay deposit: Environmental Geochemistry and Health, v. 36, p. 613–631.
- Morrison, K.D., Misra, R., and Williams, L.B., 2016, Unearthing the antibacterial mechanism of medicinal clay: A geochemical approach to combating antibiotic resistance: Nature Scientific Reports, v. 5, p. 19043, doi: 10.1038/srep19043.
- Mosier, D.L., Berger, V.I., and Singer, D.A., 2009, Volcanogenic massive sulfide deposits of the world: Database and grade and tonnage models: U.S. Geological Survey Open-File Report 2009-1034, 50 p.
- Murad, E., and Rojik, P., 2003, Iron-rich precipitates in a mine drainage environment: Influence of pH on mineralogy: American Mineralogist, v. 88, p. 1915–1918.
- 2005, Iron mineralogy of mine drainage precipitates as environmental indicators: Review of the current concepts and a case study from the Sokolov basin, Czech Republic: Clay Minerals, v. 40, p. 427–440.
- Naumov, V.B., Dorofeeva, V.A., Mironova, O.F., and Prokof'ev, V.Y., 2015, Sources of high-pressure fluids involved in the formation of hydrothermal deposits: Geochemistry International, v. 50, p. 590–606.
- National Committee for Clinical Laboratory Standards (NCCLS), 2005, Manual of antimicrobial susceptibility testing: American Society for Microbiology, QR177.M37, ISBN 1-55581-349-6, 241 p.
- Newman, D.J., and Cragg, G.M., 2007, Natural products as sources of new drugs over the last 25 years: Journal of Natural Products, v. 70, p. 461–77.
- Nordstrom, K., 1977, Thermochemical redox equilibria of ZoBell's solution: Geochimica et Cosmochimica Acta, v. 41, p. 1835–1841.
- Otto, C.C., Cunningham, T.M., Hansen, M.R., and Haydel, S.E., 2010, Effects of antibacterial mineral leachates on the cellular ultrastructure, morphology and membrane integrity of *Escherichia coli* and methicillin-resistant *Staphylococcus aureus*: Annals of Clinical Microbiology and Antimicrobials, article 9:26, 13 p. doi: 10.1186/1476-0711-9-26.
- Pevear, D.R., Williams, V.E., and Mustoe, G.E., 1980, Kaolinite smectite and K-rectorite in bentonites: Relation to coal rank at Tulameen, British Columbia: Clays and Clay Minerals, v. 28, p. 241–254.
- Pirajno, F., 2009, Hydrothermal processes and mineral systems: Berlin, Springer, 1241 p.
- Power, S.G., Field, C.W., Armstrong, R.L., and Harakal, J.E., 1981, K-Ar ages of plutonism and mineralization, western Cascades, Oregon and southern Washington: Isochron/West, v. 31, p. 27–29.
- Priest, G.R., 1990, Volcanic and tectonic evolution of the Cascade volcanic arc, central Oregon: Journal of Geophysical Research, v. 95, p. 19583–19599.
- Puigdomenech, I., 2004, Hydra/Medusa chemical equilibrium database and plotting software: Stockholm, Sweden: KTH-Royal Institute of Technology, www.kth.se/en/che/medusa/downloads-1.386254
- Repine, J.E., Fox, R.B., and Berger, E.M., 1981, Hydrogen peroxide kills *Staphylococcus aureus* by reaction with *Staphylococcal* iron to form hydroxyl radical: Journal of Biological Chemistry, v. 256, p. 7094–7096.
- Reyes, A.G., 1990, Petrology of Philippine geothermal systems and the application of alteration mineralogy to their assessment: Journal of Volcanology and Geothermal Research, v. 43, p. 279–309.
- Rimstidt, J.D., and Vaughan, D.J., 2003, Pyrite oxidation: A state of the art assessment of the reaction mechanism: Geochimica et Cosmochimica Acta, v. 67, p. 873–880.
- Schoonen, M.A.A., Harrington, A.D., Laffers, R., and Strongin, D.R., 2010, Role of hydrogen peroxide and hydroxyl radical in pyrite oxidation by molecular oxygen: Geochimica et Cosmochimica Acta, v. 74, p. 4971–4987.

- Shanks, W.C.P. III, and Thurston, R., 2012, Volcanogenic massive sulfide occurrence model: U.S. Geological Survey Scientific Investigations Report 2010-5070-C, 345 p.
- Sherrod, D.R., and Smith, J.G., 2000, Geologic map of upper Eocene to Holocene volcanic and related rocks of the Cascade Range, Oregon: U.S. Geological Survey Scientific Investigations Map I-2569.
- Singer, D.A., Berger, V.I., and Moring, B.C., 2008, Porphyry copper deposits of the world: Database, map, and grade and tonnage models: U.S. Geological Survey Open-File Report 2005-1060, 62 p.
- Srodon, J., Drits, V.A., McCarty, D.K., Hsieh, J.C.C., and Eberl, D.D., 2001, Quantitative X-ray diffraction analysis of clay-bearing rocks from random preparations: *Clays and Clay Minerals*, v. 49, p. 514–528.
- Susse, C., Epain, R., and Vodar, B., 1966, Determination de la courbe de fusion de soufre sous pression jusqu' a 90 kbars: *Journal de Chimie Physique*, v. 11–12, p. 1502–1506.
- Tanner, D., Henley, R.W., Mavrogenes, J.A., Holden, P., and Mernagh, T.P., 2015, Silica hydrate preserved with $\delta^{18}\text{O}$ -rich quartz in high-temperature hydrothermal quartz in the high sulfidation copper-gold deposit at El Indio, Chile: *Chemical Geology*, v. 391, p. 90–99.
- Taylor, B.E., and Huston, D.L., 1998, Hydrothermal alteration of oxygen isotope ratios in quartz phenocrysts, Kidd Creek mine, Ontario: Magmatic values preserved in zircons—Comment: *Geology*, v. 26, p. 763–764.
- Velde, B., 1995, Origin and mineralogy of clays: Berlin, Heidelberg, New York, Springer, 329 p.
- Velde, B., and Lanson, B., 1993, Comparison of I-S transformation and maturity of organic matter at elevated temperatures: *Clays and Clay Minerals*, v. 41, p. 178–183.
- Walker, G.W., and Macleod, N.S., 1991, Geologic map of Oregon: U.S. Geological Survey, Open File Report 03-67, scale 1:500,000.
- Walsh, C., 2000, Molecular mechanisms that confer antibacterial drug resistance: *Nature*, v. 406, p. 775–781.
- White, N.C., and Hedenquist, J.W., 1995, Epithermal gold deposits: Styles, characteristics, and exploration: *Society of Economic Geologists Newsletter* 23, p. 1, 9–13.
- Williams, L.B. and Haydel, S.E., 2010, Evaluation of the medicinal use of clay minerals as antibacterial agents: *International Geology Review*, v. 52, p. 745–770.
- Williams, L.B., and Hillier, S., 2014, Kaolins and health: From first grade to first aid: *Elements*, (*International Magazine of Mineralogy, Geochemistry and Petrology*), v. 10, p. 207–211.
- Williams, L.B., Holland, M., Eberl, D.D., Brunet, T., and Brunet de Courrou, L., 2004, Killer clays! Natural antibacterial clay minerals: *Mineralogical Society of London Bulletin*, v. 139, p. 3–8.
- Williams, L.B., Haydel, S.E., Giese, R.F., and Eberl, D.D., 2008, Chemical and mineralogical characteristics of French green clays used for healing: *Clays and Clay Minerals*, v. 56, p. 437–452.
- Williams, L.B., Metge, D.W., Eberl, D.D., Harvey, R.W., Turner, A.G., Prapaipong, P., and Poret-Peterson, A., 2011, What makes a natural clay antibacterial?: *Environmental Science and Technology*, v. 45, p. 3768–3773.
- Wilson, M.J., 2003, Clay mineralogical and related characteristics of geophagic materials: *Journal of Chemical Ecology*, v. 29, p. 1525–1547.